Lawrence Berkeley National Laboratory

Title
STRUCTURE AND PROPERTIES OF Fe-Mo-C STEELS

Permalink
https://escholarship.org/uc/item/3vj2b9qs

Author
Clark, Robert Allan.

Publication Date
1973-06-01

STRUCTURE AND PROPERTIES OF Fe-Mo-C STEELS

Robert Allan Clark
(M.S. Thesis)

June 1973

DISCLAIMER

STRUCTURE AND PROPERTIES OF Fe-Mo-C STEELS

Contents

STRUCTURE AND PROPERTIES OF Fe-Mo-C STEELS

Robert Allan Clark
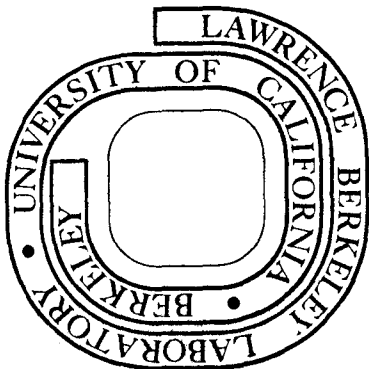
Inorganic Materials Research Division, Lawrence Berkeley Laboratory and
Department of Materials Science and Engineering, College of Engineering;
University of California, Berkeley, California

ABSTRACT

The microstructures of a series of vacuum melted Fe-Mo-C and Fe-Mo-Co-C steels were investigated using transmission electron microscopy. The correlating mechanical properties of these steels were examined by fracture toughness (K_{Ic}) tests, Charpy V-notch impact tests, tensile tests and hardness measurements. Examinations of each alloy were conducted in the as-quenched fully martensitic condition as well as martensites quenched and tempered for one hour at 400°C and 600°C. M_s temperature measurements conducted on each alloy showed that, at constant carbon content, increasing Mo content decreased the M_s temperature; however, addition of Co to a given Fe-Mo-C steel had no noticeable effect on the M_s temperature. The two 0.4% carbon steels having a high M_s temperature had approximately one-half the amount of transformation twinning associated with the two 0.4% carbon steels having higher Mo contents and lower M_s temperatures. The fracture toughness of the steels with less twinning was markedly superior to the toughness of those steels with more heavily twinned microstructures. The toughness of Fe-Mo-C steels was superior to that of similar steels containing a cobalt addition.

Steels with higher M_s temperatures exhibited more auto-tempered Fe_3C than steels with lower M_s temperatures, as expected. Tempering at 400°C resulted in Widmanstatten precipitation of Fe_3C, as well as

heavy lath boundary precipitation of Fe_3C, in all alloys. In addition, a MoC precipitate was identified in all specimens tempered at 400°C. The 600°C tempering treatment resulted in spherodization of Fe_3C precipitates and resolution of the Fe_3C as Mo_2C precipitated. Resolution of Fe_3C was most extensive in the higher Mo content steels. The Fe-Mo-C system exhibits secondary hardening with the precipitation of Mo_2C after tempering at 600°C. This secondary hardening is generally associated with a reduction in toughness. Addition of Co to Fe-Mo-C steels inhibited or eliminated the secondary hardening effect normally observed. Toughness, however, did not improve and in fact decreased with Co additions.

It is concluded that Co additions are detrimental to Fe-Mo-C steels. Based on microstructural examinations, a hypothesis as to why Co has this affect is presented. An optimum Mo content for 0.4% carbon Fe-Mo-C steels is determined from the mechanical testing data and explained by the correlating microstructural features.

I. INTRODUCTION

During the past two decades the mechanical metallurgy profession
has acquired two of its strongest techniques for continuing advancement
of the science--thin foil transmission electron microscopy and fracture
mechanics tests for determining toughness. Thin foil transmission
electron microscopy allowed, for the first time, examination of some
of the minutest microstructures and substructures present in bulk
materials. Fracture mechanics enabled the first determination of a
toughness parameter which qualifies as a material parameter. With the
advent of these techniques, metallurgists finally had the ability to
accurately correlate the mechanical properties of a material (i.e.,
strength, toughness, ductility, etc.) with the microstructure responsible
for the observed properties. Unfortunately, even subsequent to introduction
of the aforementioned techniques, a considerable amount of research has
been and still is conducted without taking full advantage of the benefits
of our new powerful methods. Many researchers still conduct myriads
of mechanical properties tests on alloys, but fail to examine the
microstructure responsible for the properties being measured. On the
other hand, there are examples of excellent microstructural examinations
of an alloy system without any information as to the physical properties
the microstructures engender. How much more useful the knowledge gained
would be if a complete job was done!

There are, of course, works which deal thoroughly and excellently
with both the physical properties and the microstructure of a system.
However, here another problem often arises. Many of the systems
investigated are commercial alloys. These alloys almost invariably are

quite complicated in the sense that numerous alloying elements are present
in the system. While it is useful to categorize the mechanical properties
and accompanying microstructures of these complicated systems, the presence
of numerous alloying elements tends to make it impossible to associate
a given microstructure with the presence, lack, or change in amount of
a given element. There are too many possible variables affecting the
microstructure and mechanical properties. Thus, a useful program to
undertake would involve a simple alloy system such as an essentially
ternary steel consisting of Fe, C and one alloying element. In such a
system, the microstructure and mechanical properties could be correlated
with the amount of the alloying element present. Such an investigation
would allow the determination of just what effects the single variable
element would have. A series of such investigations involving a different
variable each time would greatly contribute to metallurgical expertise.
Empiricism would surrender to scientific alloy design where the known
effects caused by each element could be incorporated into alloys to
yield a predetermined set of properties.

This paper deals with one effort to categorize both the microstructural
and mechanical effects of a single variable element in a simple alloy
system. The effects of varying Mo content in Fe-Mo-C alloys are explored.
In addition, the results of adding Co at the different Mo contents is
studied. This work is one of a series of similar programs under the
direction of Professor Gareth Thomas exploring the consequences of
varying single elements in simple steel systems.[1-5] Research efforts
along the same track have also been conducted by a few other investigators.[6-11]
However, the majority of investigations studying both microstructure and

mechanical properties, though often thorough and well done, have concentrated on one alloy.[12-15]

The investigation to be presented here studies the mechanical properties, yield and ultimate tensile strength, plane strain fracture toughness, hardness, etc., and accompanying microstructures of a series of Fe-Mo-C and Fe-Mo-Co-C steels. The steels are examined in their as-quenched fully martensitic condition and as martensites tempered for one hour at 400°C and 600°C. Investigation of the effects of Mo additions to steels should be interesting as it is a widely-used alloying element.[16,17] Molybdenum is a ferrite stabilizer--in other words, a gamma-loop former.[18] Thus, the choice of alloy composition was such as to allow complete austenite formation so a 100% martensitic structure could be formed in all alloys.[19]

Another interesting aspect in the study of Mo-containing steels is that Mo is a strong secondary hardener.[6,7] Secondary hardening is associated with the precipitation of a coherent[9,20-22] alloy carbide. The coherency of the precipitate creates a lattice strain in the matrix which results in a higher strength and hardness[9,23-25] but is accompanied by a reduction in the toughness.[7,15] The precipitate responsible for secondary hardening in molybdenum-containing steels has been identified to be Mo_2C.[6,7,9,22-27] Detailed investigations of the nature and identification of this precipitate have been conducted by Raynor, et al.[28] According to Irvine[7] Mo is preferred as a secondary hardening element over other secondary hardeners, notably W and V. He contends that Mo is cheaper than W and is more easily taken into solution than V. The latter is a valid point to consider. The secondary hardening mechanism

depends on an ultrafine alloy carbide precipitation, thus the elements have to be in solution for the mechanism to function. It is extremely difficult to redissolve vanadium carbides into solution after the initial casting.

A point of great interest which this investigation hopes to shed some light on is the effect of Mo additions on the amount of transformation twinning present in as-quenched martensites. Twinning has been associated with different effects on mechanical properties. While some authors regard transformation twinning as a potential strengthening mechanism[6,29] other researchers have associated marked reductions in toughness with the presence of the twins.[3,30] The effect of Mo on transformation twinning has not yet been investigated. Thus my research correlating microstructure with mechanical properties should add some useful information in this area.

This work will also add some data to other currently interesting topics. For example, what are the effects of austenite SFE and CRSS on the mode of transformation? There are currently no clear answers to these questions but data on the effects of Mo, which lowers SFE[20] and is a strong substitutional strengthener[27] should be useful. Also, the true effects of Co additions to steels are not known. Recent investigations have shown that Co which supposedly raises M_s temperature does not result in decreased twinning.[2] The effects of Co additions to two of my Fe-Mo-C steels were investigated. The result of these additions on mechanical properties and microstructure will be of definite interest.

II. EXPERIMENTAL PROCEDURE

A. Alloy Preparation

The alloys for this research program were all donated by Republic Steel. A chemical analysis of each material is given in Table I. These alloys were specially prepared using vacuum melting techniques to keep the impurity levels down. Each alloy was initially cast in 50 lb ingots. The 0.4 carbon alloys were received as nominal 0.1 in. and 0.5 in. hot-rolled plates. The 0.18 carbon alloy was received as 0.1 in., 0.5 in. and 1.0 in. hot-rolled plates. Initial heat treatment of all as-received plate consisted of first sand-blasting surfaces clean, then (in 100 lb lots) vacuum homogenizing at 1200°C for 48 hours and furnace cooling. This was done prior to any machining.

B. Specimen Machining and Heat Treatment

Three types of specimens were employed in the mechanical properties testing aspect of this research program; Charpy V-notch bars, round tensile specimens and fracture toughness (K_{Ic}) specimens. Figure 1 shows schematically in which direction each type of specimen was cut from the rolled plate. The dimensions of the finished Charpy V-notch bars are shown in Fig. 2a. These bars were completely machined to their finished state, including the V-notch, prior to any heat treating. Heat treatment of the Charpy bars consisted of austenitizing at 1200°C in an Argon atmosphere for one hour, then quenching into ice water immediately after which the specimens were placed in liquid nitrogen for one hour to ensure complete transformation to martensite.

The final dimensions of the K_{Ic} specimens used are given in Fig. 3. These dimensions were chosen so as to comply with the latest ASTM code on

fracture toughness testing.[31] Prior to heat treating the specimens were machined to the final dimensions shown except with a greater thickness and no 0.008 in. slot. After heat treating and, where applicable, tempering, the specimens were surface ground under flood cooling to their final width with at least 0.05 in. being removed from each side. This procedure ensured removal of any possible decarburized layer which could affect crack propagation. Finally, the 0.008 in. crack nucleating slot was ground in.

Figure 4 is a schematic illustration of the steps taken in preparation of specimens to test tensile properties. The final dimensions of these 1 in. gage length specimens are shown in Fig. 2b. As seen in Fig. 4, "blocks" of material the same size as K_{Ic} specimens were first cut from the same 0.5 in. nominal thickness plate as the K_{Ic} fracture toughness specimens. These "blocks" were then squared and center holes for four tensile specimens were drilled. After this initial machining, the "blocks" were heat treated. Heat treatment of K_{Ic} specimens and tensile blocks consisted of 1) austenitization at 1200°C for one hour in Ar, 2) quenching into agitated ice-10% brine, and 3) immediately refrigerating in liquid nitrogen for one hour to ensure complete transformation to martensite. After this heat treatment the tensile blocks were cut into four rectangular blanks, one about each center hole. The blanks were then wet ground to just over the final gage section diameter and the ends were threaded. All grinding was done under flood cooling conditions and at such speed as to minimize heating. Just prior to testing all tensile specimens were surface buffed along the gage section on a lathe using kerosene cooled 600 grit emery paper. This last step was done so as to remove

any scratches or possible griding marks which could act as stress-raisers during testing. Heat treating the tensile specimens in blocks the same size as fracture toughness specimens ensured as closely as possible similar cooling rates during quenching, hence similar micro-structures. This, in turn, increases the validity of any correlation between fracture toughness and tensile properties.

Every alloy was checked for complete through-hardening employing the quenching conditions previously stated. Hardness tests were made across sections of each material used, with no significant variations in hardness found. X-ray diffraction studies assured complete trans-formation to martensite. To within the usual accuracy (~2%), there was no detectable retained austenite.

Tempering of all specimens was conducted in closely controlled neutral salt baths. The heat capacity of the salt baths was much greater than that of the specimen or specimens being tempered at one time. After tempering specimens were air cooled.

C. Carbon Analysis

Carbon analyses were conducted on each alloy at three different points in the research program. The first analysis was on the plate material as received from Republic Steel. A second analysis was conducted after the homogenizing treatments. The final analysis was made from the gage sections of the tensile specimens after testing. A loss of 0.01% carbon occurred during the homogenization process. No further loss was detected in the failed samples. The values shown in Table I are those of the as-received plate.

D. Martensite Start Temperature Measurement

The M_s temperature of each alloy studied was determined. The specimens used in this experiment were several 1/2 in. × 1 in. × 0.020 in. thick coupons of each material. A typical run of the experiment involved: 1) austenitizing a coupon at 1200°C for seven minutes in an Argon atmosphere, 2) quenching directly into a neutral salt bath held at the temperature being studied, 3) after 15 seconds in the first salt bath rapidly upquenching the coupon into a second neutral salt bath held at a considerably higher temperature, 4) after one hour in the high temperature salt bath, quench the coupon in ice-brine, and 5) metallo-graphically polished and etch the specimen and observe the surface using a metallograph. The very thin coupons (0.020 in. thick) were used to ensure almost instantaneous attainment of thermal equilibrium during the quenching steps. A carbon analysis of these coupons before and after the experiment showed no decarburization. The initial quenching step is to a trial M_s temperature, the first such temperature for each alloy being near its calculated M_s temperature. The upquenching step is used to temper any martensite that may have formed during the initial quench step. The temperature of this tempering bath was 600°C for alloys 214, 215 and 198 and 650°C for alloys 216 and 217. These temperatures were chosen to be in the metastable austenite bay between the pearlite and bainite noses for each alloy. Thus one could temper for a reasonable length of time without worrying about complicating transformations. Quenching the coupon from the tempering bath into ice-brine resulted in a 100% martensitic structure. The coupons were then wet ground on a belt sander to approximately half thickness. After

this a standard metallographic polishing sequence was used down to a one micron diamond wheel. Next the samples were etched in 5% nital, then examined with a Carl Zeiss Metallograph. If the initial quench from the austenitizing temperature was to a temperature below the M_s temperature, the martensite plates formed during this quench were subsequently tempered. These tempered martensite plates were quite distinct from the untempered martensite formed during the ice-brine quench. If the initial quench from the austenitizing temperature was to a temperature above the M_s temperature, no contrast variations were distinguishable in the coupon. Thus it could readily be determined if the initial quenching bath was at a temperature above or below the material's M_s temperature, and the temperature of this bath could then be lowered or raised 25°C for the next trial run. In this manner, the M_s temperature of each alloy was bracketed, e.g., a lower and upper limit encompassing each M_s temperature was found. Subsequently, a binary search was conducted within each bracket to determine each M_s temperature to within ±5°C. The measured M_s temperatures are listed in Table I.

It should be noted that the measured M_s values are considerably higher than those one would obtain by calculation using the standard formulae. It is believed that this result is due to the large grain size attained by austenitization at 1200°C. This result would be in agreement with conclusions reached by Breinan and Ansell[32] on the effect of austenite yield strength on M_s temperature.

E. Mechanical Testing

1. Charpy Impact Testing

The Charpy V-notch specimens shown in Fig. 2a were used. All tests were conducted at room temperature (23°C). Testing was conducted on a Sonntag Universal impact testing machine with a 224 ft-lb capacity. At least two tests were run for each heat treatment condition. The impact values reported are averages of those tests.

2. Plane Strain Fracture Toughness (K_{Ic}).

Figure 3 shows the specimens used for these tests. Different thickness specimens were employed so that the plane strain criterion: $B \geqslant 2.5(K_{Ic}/\sigma_{ys})^2$ where B = specimen width was always assured.[31] All tests were conducted at room temperature, 23°C, on a 300 kip capacity MTS machine. Prior to testing, all specimens were fatigued at a rate of 6 Hz until a fatigue crack between 0.05 in. and 0.10 in. long was visible on each side of the specimen. Loading of the specimen during fatiguing was such that the proper fatigue crack length resulted between 20,000 and 30,000 cycles. Specimens were ultimately pulled at a head speed of 0.3 cm/min. Specimen design and all fracture toughness tests were conducted in accordance with ASTM specifications.[31]

3. Tensile Properties and Percent Elongation

Tensile testing was conducted on a 300 kip capacity MTS machine. The hydraulic ram head speed was 0.3 cm/min. All testing was conducted at room temperature (23°C) with at least two tests of each heat treatment condition. Values reported are averages of all tests. Elongation (plastic deformation at failure) was determined from a set of gage marks inked with a vernier height gage onto each specimen

prior to testing. Measurements of each gage section before and after testing were accurately determined using an optical microscope equipped with a vernier translating stage calibrated to 0.001 in. Measurement of the gage section along exactly the same point on each specimen's diameter, before and after testing, was assured by inking a center line onto each specimen at the same time the gage marks were placed. Values of percent elongation reported are averages of at least two tests.

4. Hardness

Rockwell "C" hardness values were obtained for the materials in their "as-quenched" condition. Hardness specimens were cut from previously tested K_{Ic} specimens in such a manner as to avoid the work hardened zone caused during fatigue-cycling. Prior to hardness testing the surfaces were prepared using standard metallographic polishing techniques. At least 10 indentations were made in each specimen, the hardness values reported being an average of all tests.

F. Microscopy

1. Optical Metallography

Optical microscopic examination was conducted on heat-treated sample bars of each alloy for each heat treatment condition. Specimens were prepared by wet grinding successively on 120, 240, 320, 400 and 600 grit papers and then polishing on a one micron diamond wheel lubricated with kerosene. A 2% nital etch was used. Pictures were taken using oil immersion techniques on a Carl Zeiss Optical Metallograph.

2. Fractography

All fracture surfaces of Charpy impact bars and K_{Ic} specimens were examined using a JSM-U3 Scanning Electron Microscope operated at 25 kV in a back-scattered electron mode. Fracture surfaces were protected with acetate-replicating tape while the specimens were being cut to an acceptable size for viewing.

3. Transmission Electron Microscopy

Microstructural examinations using thin foils were conducted for each alloy-heat treatment condition. Transmission electron microscopy was conducted on a Siemens Elmiskop IA electron microscope operated at 100 kV and on a Hitachi high voltage electron microscope operated at 650 kV.

Foils for transmission electron microscopy were prepared in the following manner:

a. 0.070 in. slices were cut out of previously tested K_{Ic} specimens perpendicular to the crack propagation direction. Cutting was done on a flood cooled Dimet saw to prevent heating. Temperatures attained during this cutting operation were tested using a thermocouple epoxied into a hole drilled into a sample specimen prior to cutting. Results of these tests indicated no possible tempering of the foils.

b. The surfaces of each slice were wet ground until parallel. Again, low rates of feed were used to prevent heating, less than 0.0005 in. being removed per pass.

c. The parallel slices were chemically thinned to 0.005 in. in a hydrogen-peroxide hydroflouric acid solution. This solution had to be frequently changed (every 15 minutes) and kept below 30°C. At the conclusion of this step, specimen thickness did not vary by more than 0.001 in. from one end to the other.

d. Final thinning was by electropolishing in a chromic-acetic acid solution of the following composition:

$$88 \text{ gm } CrO_3$$
$$470 \text{ ml } HAc$$
$$35 \text{ ml } H_2O$$

Electropolishing was conducted using the window method with the solution at 10°C and an applied bias of 10 to 12 volts. The specimen was so masked as to produce foils in several different regions. Thus foils from several different regions of a K_{Ic} specimen could be obtained from each original slice.

III. RESULTS AND DISCUSSION

A. Transmission Electron Microscopy--Summary of Findings

The microstructure of each of my alloys in each of the heat

treatment conditions studied was examined using transmission electron

microscopy techniques. During the course of the examination several

hundred pictures were taken. Thus, the figures introduced here represent

typical structures observed, or in certain instances, where mentioned,

are designed to illustrate specific points of interest. Typically,

the 0.4 carbon alloys (214, 215, 216 and 217) in the as-quenched condition

exhibited a mixture of dislocated lath martensite and twinned plate

martensite. Due mainly to the fact that the amount of twinning observed

in any one picture is strongly dependent on the foil orientation, it

was found impossible to assign an exact percentage to the relative

amount of twinned martensite in any one alloy. However, after careful

visual examination of many pictures of each alloy it is apparent that

alloys 214 and 215 have about the same amount of twinning. Also, alloys

216 and 217 have close to the same amount of twinning. However, the

first mentioned pair (214 and 215) exhibit approximately twice as

much twinned area as the latter pair (216 and 217). Alloy 198, the

low carbon alloy, is almost 100% dislocated martensite. Investigation

for retained austenite was conducted, especially on alloy 216 which

exhibited superior mechanical properties, but no evidence of retained

austenite was found. All of the as-quenched structures exhibited some

auto-tempered Fe_3C. A further point to note is that the two alloys

containing Co, 215 and 217, appeared to have, on the average, a finer

structure, i.e., thinner laths and plates, than the similar alloys

without Co. This obviously results in an increase in boundary area

for the Co containing steels.

Tempering at 400°C resulted in both a matrix and lath boundary

precipitation of Fe_3C. There was also cementite precipitation at the

matrix-twin interfaces as previously reported by other researchers.[1-4,33]

Analysis of streaks in the diffraction patterns led to the conclusion

that very small amounts of MoC were also present in all the alloys

with this tempering treatment. However, I was unable to uniquely

image this precipitate. This type of precipitate has also been noted

by previous researchers.[12,26]

Tempering at 600°C resulted in a very fine precipitation of the

Mo_2C alloy carbide associated with secondary hardening. Precipitation

of this phase was accompanied by dissolution of the previous cementite

precipitate. Some cementite was still present in the 0.4 C alloys though

none was observed in the 0.18 C alloy. Also, the low Mo alloys 216

and 217 appeared to have more remaining Fe_3C than the higher Mo alloys

214 and 215. The remaining cementite had considerably spherodized

so that it no longer existed as a continuous interlath precipitate.

1. Structure of As-Quenched Martensite

The typical microstructures of alloy 198 in the as-quenched condition

is shown in Fig. 5. This material is the only low carbon alloy

(0.18 wt%) in the series of compositions studied. Its microstructure

is predominantly a fine dislocated lath martensite as shown in Fig. 5a.

The laths are mainly of the order of 0.25-0.50 microns wide; however,

a few much thicker laths, up to 2 microns wide, as shown in Fig. 5b,

are also present. There is evidence of auto-tempering in both 5a and

Fig. 5b. By trace analysis, the carbide product was seen to lie along

{110} planes, thus it is probably Fe_3C. Figure 5c is a {110} dark field

of the same area as Fig. 5b and lights up one variant of the auto-

tempered carbide. An extremely small amount of twinned martensite

plates were also present. Also, in a small percentage of the regions

observed, fine interlath carbides were present.

Figures 6a, 6b and 6c show the typical microstructure of as-quenched

alloy 214. This structure consists of a mixture of heavily dislocated

lath martensite together with a substantial amount of twinned martensite.

The amount of twinning visible, however, is by no means constant from

region to region as a comparison of Figs. 6a and 6c will show. These

pictures were taken from different areas of the same foil. Figure 6b

is a dark field of Fig. 6a and shows the presence of an interlath

carbide precipitate. Calculation of the camera constant and the

resulting d-spacings from several carbide spots determined that this

carbide is Fe_3C. In general, very little auto-tempered carbide was

present in the laths of plates; only the interlath boundaries con-

sistently showed a precipitate.

Alloy 215 has a composition very similar to that of alloy 214, as

shown in Table I, with the exception that 9% Co has been added to 215.

The as-quenched structure of 215 is represented in Figs. 7 and 8. The

structure consists of extremely fine (~0.1μ wide) heavily dislocated

laths mixed with fine (~0.2μ wide) heavily twinned plates. In some

regions, as shown in Figs. 7a and 7b, the fine laths appear to be quite

randomly mixed together. Close examination of some of the larger laths

in these figures will reveal that they actually are a number of fine

parallel laths.   In other areas the fine laths exist in large families

or packets as seen in Fig. 7c.   Each family has the same basic orientation,

but adjacent laths in a packet are occasionally twin related or separated

by a small angle boundary.[34]   Figure 7d is a dark field of 7c lighting

up one particular packet of laths.   Figure 8 shows a heavily twinned

region in the microstructure.   Figure 8a is a bright field picture

while 8b is a dark field of a twin spot, hence the twins reverse contrast.

Note, here again, some regions of a foil show little or no twinning

while other regions appear heavily twinned.   In some instances the

foil orientation could strongly affect the amount of twinning observed;

however, several orientations of a given region were often observed to

obtain a maximum amount of information.   Small amounts of auto-tempered

carbides were found in this alloy also.   They appeared to be almost

exclusively in the interlath boundaries between different packets of

laths.   No carbides were visible in the boundaries between laths within

a packet.   There does not appear to be any significant auto-tempered

carbides within the laths themselves.   However, due to the fineness

of these laths it was not possible to determine this rigorously.

Another effect of having numerous extremely fine laths in many orientations

was horrendous diffraction patterns even using the smallest selected area

apertures.   Thus, it was not possible to determine the nature of the

carbide precipitate; however, there is no reason not to believe it is

Fe_3C as determined in alloy 214.

The next Figures, 9a and 9b, show the microstructures typical of

as-quenched 216.   The microstructure here is similar to that seen in

alloy 214.   It consists mainly of dislocated lath martensite with lath

size ranging from 0.1μ to 0.5μ wide. The amount of twinning present
in this alloy is considerably less than that in 214. There are, however,
still some regions that exhibit heavy twinning. Most regions show little
or no twinning. Auto-tempering was minimal in this alloys. Some
precipitation inside laths was identified as Fe_3C by trace analysis.
Also, a few Fe_3C precipitates were observed in the lath boundaries as
seen in Fig. 9b. However, this auto-tempering was neither widespread
throughout the structure nor in great amounts.

Alloy 217 exhibited a similar structure to 215 as did alloy 216
to 214. This is interesting because alloy 217 bears a relationship
to 216 similar to that between 215 and 214. Alloy 217 is chemically
similar to 216 except that the former has a Co addition while the latter
does not. It will be recalled that 215 has Co while 214, which is
otherwise the same chemically, does not. The structure of 217 is
predominantly very fine lath martensite, very similar to that found in
215. Figures 10a and 10d show this structure. No regions with extensive
twinning were observed, but some of the very fine ($\sim$0.1-0.2μ wide) plates
were seen to be internally twinned. Of considerable interest is the
precipitate observed in this structure. Figures 10b and 10c are both
dark fields of Fig. 10a. It will be noted that there is extensive
interlath carbide precipitation. Both spots used for these figures had
calculated d-spacings that identify Fe_3C as the precipitate. This alloy
exhibited the most extensive boundary precipitation of any of the alloys
observed. In addition, some auto-tempered Fe_3C was found in the larger
laths.

2. Structure of Martensite Tempered at 400°C

The structure of alloy 198 was not greatly changed by this tempering treatment. The main difference between the tempered and as-quenched microstructures was an increase in the amount and distribution of a Widmanstatten Fe_3C precipitate (Fig. 11a). Figure 11b is included to show that even in this low carbon martensite some twins exist. Typically the twin-matrix interface is a preferrential position for carbide nucleation, thus there is usually an Fe_3C precipitate along the interface after tempering. Even after the tempering treatment a negligible amount of interlath carbide was observed in this alloy.

The four 0.4 carbon alloys behaved quite similarly on tempering. A large amount of Widmanstatten cementite precipitated throughout the laths. There was also precipitation on twin-matrix interfaces and a further precipitation on lath boundaries. Figures 12 through 14 show typical structures of the alloys in this tempered condition. One should note in Fig. 13 the fair amount of spherodization of carbide that has occurred in alloy 215. This same effect is noticeable to a lesser extent in alloy 214 shown in Fig. 12. Alloy 217 behaved in a manner analogous with 215. The behavior of alloy 216 is illustrated in Figs. 14a, 14b, 14c and 14d. Large Widmanstatten carbides form throughout the matrix (Figs. 14a and 14b) and Fe_3C precipitates in the twin matrix interfaces (Figs. 14c and 14d).

Also noted at the 400°C tempering temperature was the presence of an MoC precipitate. However, the amounts were so miniscule as to make imaging impossible. The carbide phase was identified in each alloy by taking over-exposed diffraction patterns. In these diffraction patterns faint ring patterns were discernible. Using the camera constant

calculated for a diffraction pattern and measuring the radii of the ring patterns d-spacings were calculated. In each case the calculated d-spacings correspond to those of MoC.

3. Structure of Martensite Tempered at 600°C

The 600°C tempering temperature was chosen because previous researchers[7,15] have shown that for a one hour tempering treatment this temperature results in peak secondary hardening for the Fe-Mo-C system within approximately my composition ranges. Secondary hardening in this system is associated with coherent precipitation of the Mo_2C carbide.[9,20-22] After overaging this carbide tends to assume a needle-like shape;[22,24,25] however, one hour at 600°C is neither a long enough period nor a high enough temperature to result in substantial overaging. Thus one expects to find a fine-barely resolvable network of Mo_2C such as previously observed by Pickering[9] and others.[14]

All of the alloys examined exhibited a very fine cloud-like Mo_2C precipitate. The precipitate was identified by the directions of streaking in the diffraction patterns after the analysis of Dyson, Raynor, et al.[28] An example of a streaked diffraction pattern is shown in Fig. 15. Dark fields of the Mo_2C precipitate were taken by including the streak within the area of the objective aperture. Typical examples of the observed Mo_2C precipitate are shown in Figs. 16c and 17b.

No cementite was found in alloy C198 after the 600°C temper. The 0.4 carbon alloys, on the other hand, still contained some matrix and interlath Fe_3C. The amounts of Fe_3C varied, alloys 214 and 215 showing fair amounts (Fig. 18) and alloys 216 and 217 just minimal amounts and only in occasional locations (Fig. 16b).

B. Mechanical Properties Tests

Each alloy was subject to four tests to determine its mechanical properties. Tensile tests, plane-strain (K_{Ic}) fracture toughness tests, Charpy V-notch impact tests and hardness tests were conducted in the manners previously stated. From these tests information on yield strength, ultimate tensile strength, ductility, fracture toughness, impact toughness and hardness was obtained. The tensile test data is summarized in Table II and Figs. 19 and 20. All data represents average values from two or more tests in each condition. From the plot of yield strength vs tempering temperature (Fig. 19) one observes the characteristic secondary hardening peak for 600°C tempering of alloys 214, 216 and 198. Note, however, that alloys 215 and 217, those containing Co, do not exhibit a secondary hardening phenomenon. Since secondary hardening in Fe-Mo-C steels is associated with a coherent precipitation of Mo_2C it appears that Co either inhibits this precipitation or affects the coherency and hence the lattice strains associated with precipitation of the Mo_2C phase. Upon examining the percent elongation data in Table II, one notes that at the 600°C tempering level alloys 216 and 217, the low Mo alloys, show fair amounts of ductility. This suggests that these alloys may be starting to overage. Irvine[7] and Pickering[9] have found that higher Mo levels move the tempering temperature for peak secondary hardening to higher levels.

Results of the plane-strain fracture toughness tests are summarized in Table III and Fig. 21. All test results reported are valid K_{Ic} values in accordance with the testing criteria described earlier. The values are all averages of at least two tests. Multiple tests

characteristically exhibited extremely little scatter. Examining the

data in Table III, one notes that in all alloys, except 217, the

toughness drops at the 600°C tempering condition. This observation

is in agreement with previous researchers[12,14,15,35] who have also found

that fracture toughness decreases around the secondary hardening peak.

This drop in toughness is attributed to the strained nature of the matrix

containing a coherent or semi-coherent precipitate. The behavior of

alloy 217 may be attributed to an inhibition of the secondary hardening

precipitate Mo_2C caused by Co. However, alloy 215, which contains less

Co than 217, does not exhibit this effect. Other noteworthy points include

the fact that the alloys without Co addition are always tougher than

the comparable alloy containing Co; i.e., 214 is always tougher than

217. Thus Co is definitely detrimental to toughness. A final and

important point is that the more heavily twinned martensites, those of

alloys 214 and 215, have lower toughness than the less twinned martensites

of alloys 216 and 217. A good idea of the effect of twinning can be

obtained by comparing, in the as-quenched condition, alloy 214 and 216

and alloy 215 with 217, thus limiting the effect of Co in the comparison.

Figures 22 and 23 present the fracture toughness, K_{Ic}, of the alloys

as a function of tensile yield strength and ultimate tensile strength

respectively. These figures allow easy comparison of the materials in

their different heat treated conditions to determine the optimum

combinations of fracture toughness and tensile properties. From the

figures one notes that the alloy 216 in the as-quenched and 400°C

tempering condition exhibits the best combination of properties. A

combination of alloy 216 with other common alloys is presented in

Fig. 24. One notes that 216 without employing a thermal-mechanical treatment has properties just below those of the maraging steels.

The impact toughness as determined by Charpy V-notch tests is presented in Fig. 25. All tests were conducted at room temperature, 23°C, and the results shown represent an average of at least two tests for each alloy-heat treatment combination. Little scatter was observed in multiple tests of similar specimens. The Charpy impact toughness results, it will be noted, follow similar trends to the K_{Ic} plane strain fracture results. The main point to consider from the data, though, is that all the impact toughness values are low. Eleven ft-lbs is the maximum energy absorbed for any alloy-heat treatment combination. This low impact toughness is characteristic of low alloy high yield strength steels.

Hardness tests were conducted only on as-quenched samples of the alloys. These tests were used to ascertain two points. First, complete through hardening of the largest thickness used for each alloy was ascertained by lack of a hardness gradient between the center and outer portions of the specimen. Second, the hardness values obtained were used as an additional check on decarburization. The values recorded all correlated well with accepted hardness values for steels containing the amount of carbon which my alloys did.[36] The hardness values are reported in Table III.

C. Fractography

Scanning electron fractography was conducted on all fracture toughness specimens. The observed fracture surfaces were all remarkably similar. Figure 26 illustrates this typical fracture structure. The fracture surfaces invariably consisted of low level and small dimples mixed with varying amounts of flat cleavage-like areas. This structure is analogous with the one treated by Low in his paper.[37] In this paper, he describes how such a dimpled rupture surface, generally associated with ductile failure, can be obtained in the brittle failure of a high strength alloy. The dimpled surface is explained in terms of a coalescence mechanism during fracture. The fractographs of the alloys examined in this research project tend to support Low's proposed mechanism.

IV. CONCLUSIONS

The effects on microstructures and correlating physical properties
of two different alloying elements have been studied. First, a set of
essentially ternary Fe-Mo-C steels were examined. The effect of
increasing Mo content at a constant carbon level and the effect of varying
the amount of carbon at a given Mo content were studied. Next, a
fourth element, Co, was added to two of the steels to determine the
consequences of such an addition at different levels of Mo content.
The carbon content was kept constant at 0.4% in this latter case. The
conclusions arrived at from examination of the physical properties and
the microstructures responsible for the physical properties of these
alloys are:

1. Cobalt does not raise the M_s temperature in these alloys.
Cobalt may shift the position of and broaden the γ-loop present in this
alloy system but it does not raise the minimum temperature of austenite
stability for the compositions examined.

2. Cobalt additions do not result in any noticeable decrease in
the amount of twinning present when compared with a similar Fe-Mo-C
alloy without Co additions.

3. The presence of Co in an alloy appears to induce a finer
martensitic microstructure when the alloy is quenched to a 100% martensite
condition.

4. Addition of Co to an Fe-Mo-C steel in the "as-quenched" condition,
all other things remaining constant (i.e., other alloying elements,
heat treatment, etc.), results in a lower plane strain fracture toughness
and a slightly lower yield and ultimate tensile strength. In addition,
the ductility is considerably reduced by the Co addition.

5. Cobalt additions to Fe-Mo-C steels in as-quenched and tempered condition appear to strongly inhibit the secondary hardening reaction characteristic of Mo alloy steels. In addition, the Co containing steels have lower fracture toughness, yield and ultimate tensile strength, and lower ductility when compared to similarly tempered non-cobalt bearing steels.

6. A possible explanation of the effects of Co lies in the fine martensitic microstructure present in the Co containing alloys. These alloys also contained the greatest amounts of interlath Fe_3C precipitation. Thus Co may act to stabilize Fe_3C. Also greater amounts of interlath carbides could act as fracture paths lowering toughness. In addition, a stabilized Fe_3C would hinder the uniform precipitation of the secondary hardening Mo_2C phase by preventing a homogeneous solution of C in the iron matrix.

7. Increasing amounts of Mo, at contant C content, result in increased amounts of twinning.

8. It could not be determined if the increase in twinning was due to increased Mo content or due to a lowering of the M_s temperature caused by the addition of more Mo.

9. Microstructures with more twinning were less tough and less ductile than those microstructures exhibiting lesser amounts of twinning. Yield and ultimate tensile strengths were not greatly affected by increasing Mo additions beyond approximately 2%.

10. Lowering C content at a constant Mo level results in a substantially reduced amount of twinning. As-quenched toughness is increased as is ductility with lower C content; however, ultimate and yield tensile strengths are drastically reduced as expected.

Optimum properties were obtained with alloy 216, containing 2.2% Mo, 0.4% carbon. This alloy has enough Mo for adequate hardenability. At the same time there is not so much Mo as to attain a strong secondary hardening peak upon tempering at 600°C. Since a strong secondary hardening peak is generally accompanied by a sharp drop in toughness, this alloy benefits from only the mild secondary hardening reaction. Thus, while tensile and yield strength do drop somewhat upon tempering one hour at 600°C the loss is compensated by a much better plane strain fracture toughness than exhibited by higher Mo steels with strong secondary hardening peaks. Also, in the "as-quenched" condition, higher Mo steels would exhibit more twinning in their microstructures and this again would result in lower toughness, here without the benefit of increased tensile strengths.

ACKNOWLEDGEMENTS

REFERENCES

1. S. K. Das and G. Thomas, Trans. ASM 62, 659 (1969).

2. M. Raghavan and G. Thomas, Met. Trans. 2, 3433 (1971).

3. D. Huang and G. Thomas, Met. Trans. 2, 1587 (1971).

4. J. McMahon, Structure, Strength and Toughness of Fe/Cr/C Martensitic
   Steels (M. S. Thesis), LBL-1181, December 1972.

5. G. Thomas, Met. Trans. 2, 2373 (1971).

6. K. J. Irvine, J. Iron and Steel Inst. 200, 820 (1962).

7. K. J. Irvine, Heat Treatment of Metals, ISI Special Report No. 95
   (The Iron and Steel Institute, London, 1966) p. 37.

8. K. J. Irvine, F. B. Pickering and J. Garstone, J. Iron and Steel
   Inst. 196, 66 (1960).

9. F. B. Pickering, Precipitation Processes in Steels, ISI Special
   Report No. 64 (The Iron and Steel Institute, London, 1959) p. 23.

10. G. E. Pellissier, Engineering Fracture Mechanics 1, 55 (1968).

11. C. L. Magee and R. G. Davies, Acta Met. 19, 345 (1971).

12. C. R. Simcoe and A. E. Nehrenberg, Trans. ASM 58, 378 (1965).

13. Y. H. Liu, Trans. ASM 62, 55 (1969).

14. C. R. Simcoe, A. E. Nehrenberg, V. Biss and A. P. Coldren, Trans.
    ASM 61, 834 (1968).

15. R. Goolsby, Relationships Between Microstructure and Fracture Toughness
    in a Secondary Hardening Steel (Ph. D. Thesis), LBL-405, November 1971.

16. R. S. Areher, J. Z. Briggs and C. M. Loeb, Jr., Molybdenum: Steels-
    Irons-Alloys (Climax Molybdenum Co., 1948).

17. L. Colombier, Molybdenum in Stainless Steels and Alloys (Climax
    Molybdenum Co., Ltd., 1967).

18. E. C. Bain and H. W. Paxton, Alloying Elements in Steel (American Society for Metals, Ohio, 1961).

19. E. C. Rollason, Fundamental Aspects of Molybdenum on Transformation of Steel (Climax Molybdenum Co., Ltd.).

20. R. W. K. Honeycombe, Trans. Iron and Steel Inst. of Japan 6, 217 (1966).

21. P. Payson, Trans. ASM 51, 60 (1959).

22. P. Wilkes, Metal Science Journal 2, 8 (1968).

23. R. G. Baker and J. Nutting, Precipitation Processes in Steels, ISI Special Report No. 64 (The Iron and Steel Institute, London, 1959) p. 1.

24. R. W. K. Honeycombe, Proceedings of the National Research Institute for Metals, Tokyo, 1966, p. 44.

25. K. J. Irvine and F. B. Pickering, J. of Iron and Steel Institute 194, 137 (1960).

26. Kehsin Kuo, J. of Iron and Steel Institute 173, 363 (1953).

27. R. W. K. Honeycombe, Low Alloy Steels, ISI Publication No. 114, (The Iron and Steel Institute, London, 1968) p. 65.

28. D. J. Dyson, S. R. Keown, D. Raynor and J. A. Whiteman, Acta Met. 14, 867 (1966).

29. P. M. Kelley and J. Nutting, Proc. Roy, Soc. London A259, 45 (1960).

30. O. Johari and G. Thomas, Trans. ASM 58, 563 (1965).

31. Annual Book of ASTM Standards, Designation E399-70T, 911 (1970).

32. E. M. Breinan and G. S. Ansell, Met. Trans. 1, 1513 (1970).

33. A. J. Baker, P. M. Kelley and J. Nutting, in Electron Microscopy and Strength of Crystals, G. Thomas and J. Washburn, eds. (John Wiley and Sons, N. Y., 1963) p. 899.

34. G. Krauss and A. R. Marder, Met. Trans. $\underline{2}$, 2343 (1971).

35. B. R. Banerjee, J. Iron and Steen Institute $\underline{203}$, 166 (1965).

36. B. S. Lement, B. L. Averbach, M. Cohen, Trans. Amer. Soc. Metals $\underline{46}$, 851 (1954).

37. J. R. Low, Jr., Engineering Fracture Mechanics $\underline{1}$, 47 (1968).

Table I. Alloy compositions and M_s temperatures.

Alloy	C	Mn	Si	Mo	Co	M_s Calculated °C	M_s Measured °C
C198	0.18	0.30	0.15	3.85	---	371	356
C214	0.41	0.35	0.15	4.2	---	282	345
C215	0.43	0.34	0.15	3.85	9.0	366	345
C216	0.43	0.33	0.15	2.2	---	316	474
C217	0.42	0.33	0.15	2.1	5.2	366	474

Table II. Tensile test summary.

Type	Specimen	Average Tensile Yield Strength (psi)	Average Ultimate Strength (psi)	Percent Elongation
214	AQ	257,000	322,000	2.03
214	400	205,000	251,000	7.1
214	600	271,000	279,000	0.6
215	AQ	246,000	283,000	1.6
215	400	257,000	278,000	1.0
215	600	198,000	198,000	0.2
216	AQ	258,000	311,000	2.5
216	400	197,000	230,000	5.8
216	600	206,000	223,000	10.7
217	AQ	253,000	306,000	1.6
217	400	248,000	277,000	3.1
217	600	240,000	253,000	2.5
198	AQ	160,000	198,000	12.6
198	400	153,000	183,000	13.9
198	600	193,000	205,000	8.5

Table III. Toughness and hardness data.

Alloy	Heat Treatment	K_{Ic}	Charpy	Hardness
C198	AQ	93.2	11.1	42.5
	200°C	----	8.2	
	400°C	88.9	9.9	
	600°C	46.1	5.2	
C214	AQ	44.2	4.1	58.6
	200°C	----	7.6	
	400°C	64.1	8.2	
	600°C	41.9	3.5	
C215	AQ	35.0	4.1	57.8
	200°C	----	4.7	
	400°C	33.9	4.7	
	600°C	26.8	4.6	
C216	AQ	53.6	4.7	58.0
	200°C	----	7.6	
	400°C	94.3	11.0	
	600°C	73.3	8.7	
C217	AQ	44.1	5.3	57.7
	200°C	----	8.1	
	400°C	52.1	6.4	
	600°C	59.9	5.8	

ROLLING DIRECTION

K_{IC} SPECIMEN

CHARPY
V-NOTCH SPECIMEN

ROUND
TENSILE SPECIMEN
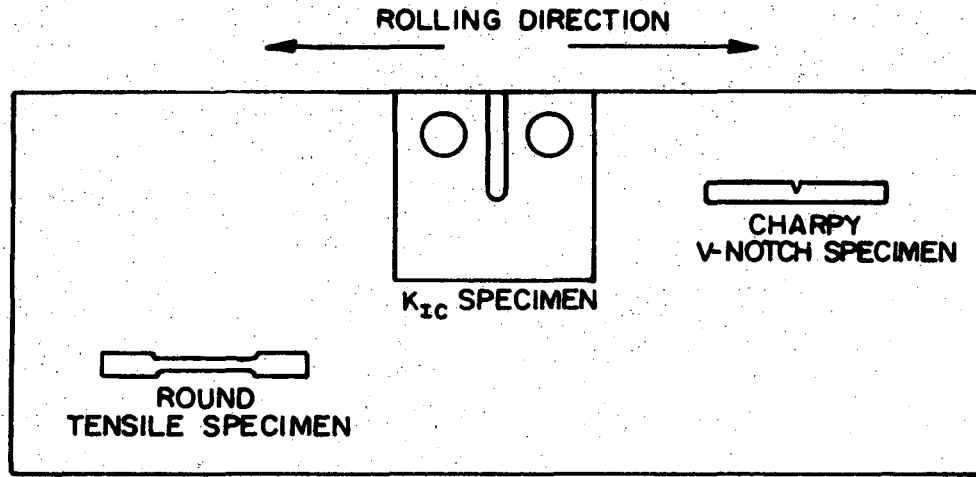
XBL 735-6188

Fig. 1.   Schematic of how mechanical properties test specimens
were cut from rolled plate.
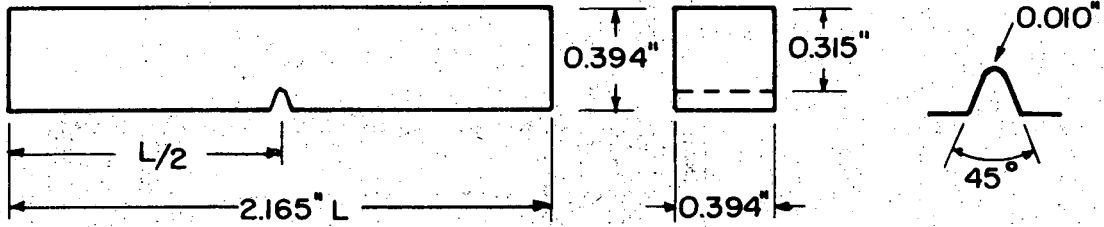
(a) CHARPY V-NOTCH IMPACT SPECIMEN
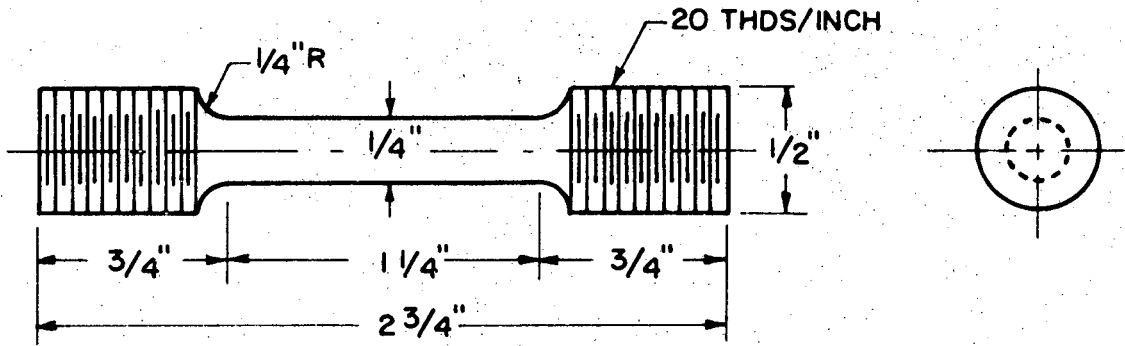
(b) ROUND TENSILE SPECIMEN

XBL 735-6189

Fig. 2
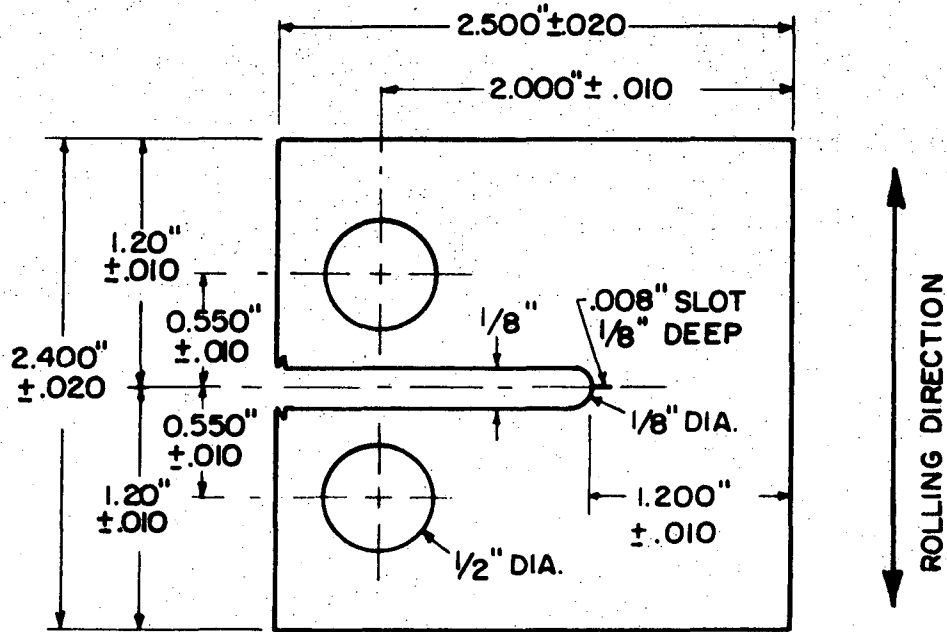
XBL 735-6190

Fig. 3. Crackline loaded fracture toughness specimen.

ROUGH TENSILE BARS, READY FOR GRINDING
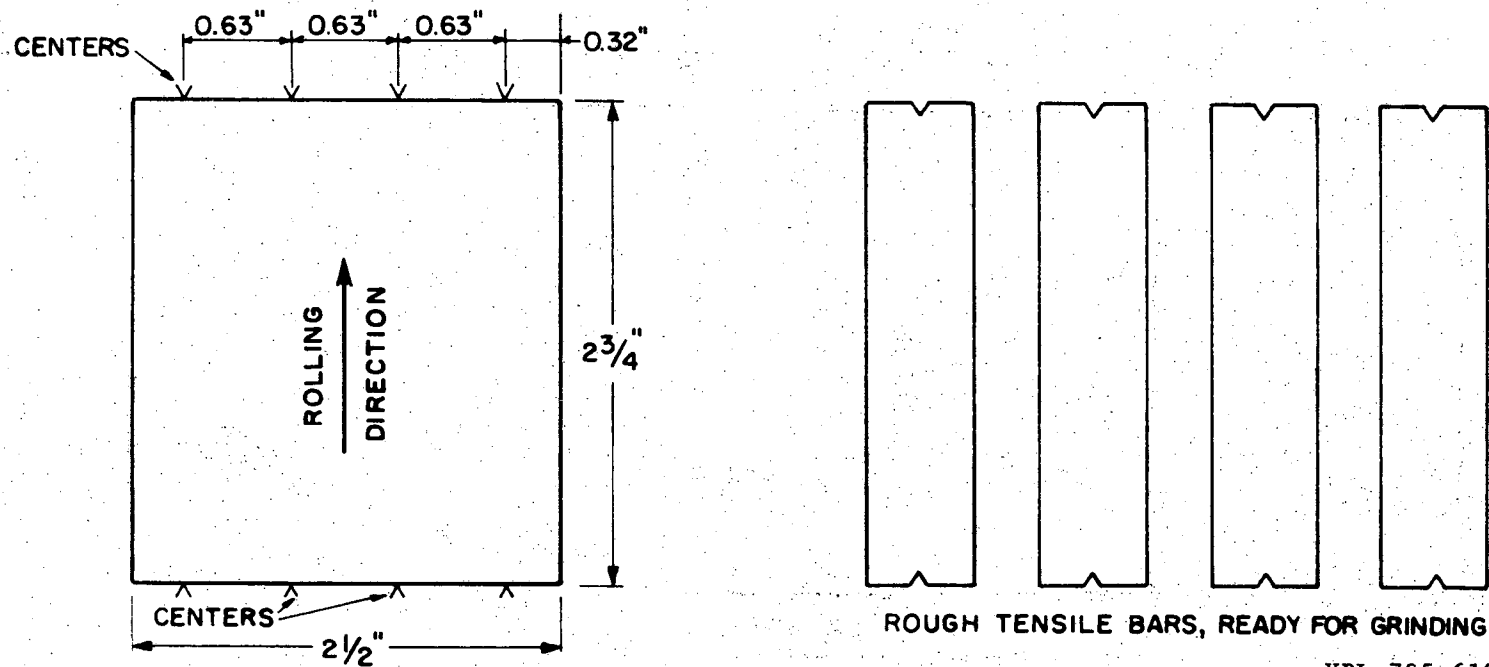
XBL 735-6191

Fig. 4. Preparation of round tensile specimens.
   A. A 2 1/2 in. × 2 3/4 in. blank is cut from the homogenized material.
   B. Center holes for four tensile specimens are drilled into each blank.
   C. The blank is heat treated to the martensitic condition.
   D. The blank is cut into four rough bars.
   E. The bars are ground to the finished tensile specimens shown in the figure.
   F. Tempering is done on finished specimens.
   Note: All cutting and grinding after step C is done using flood cooling to prevent heating.
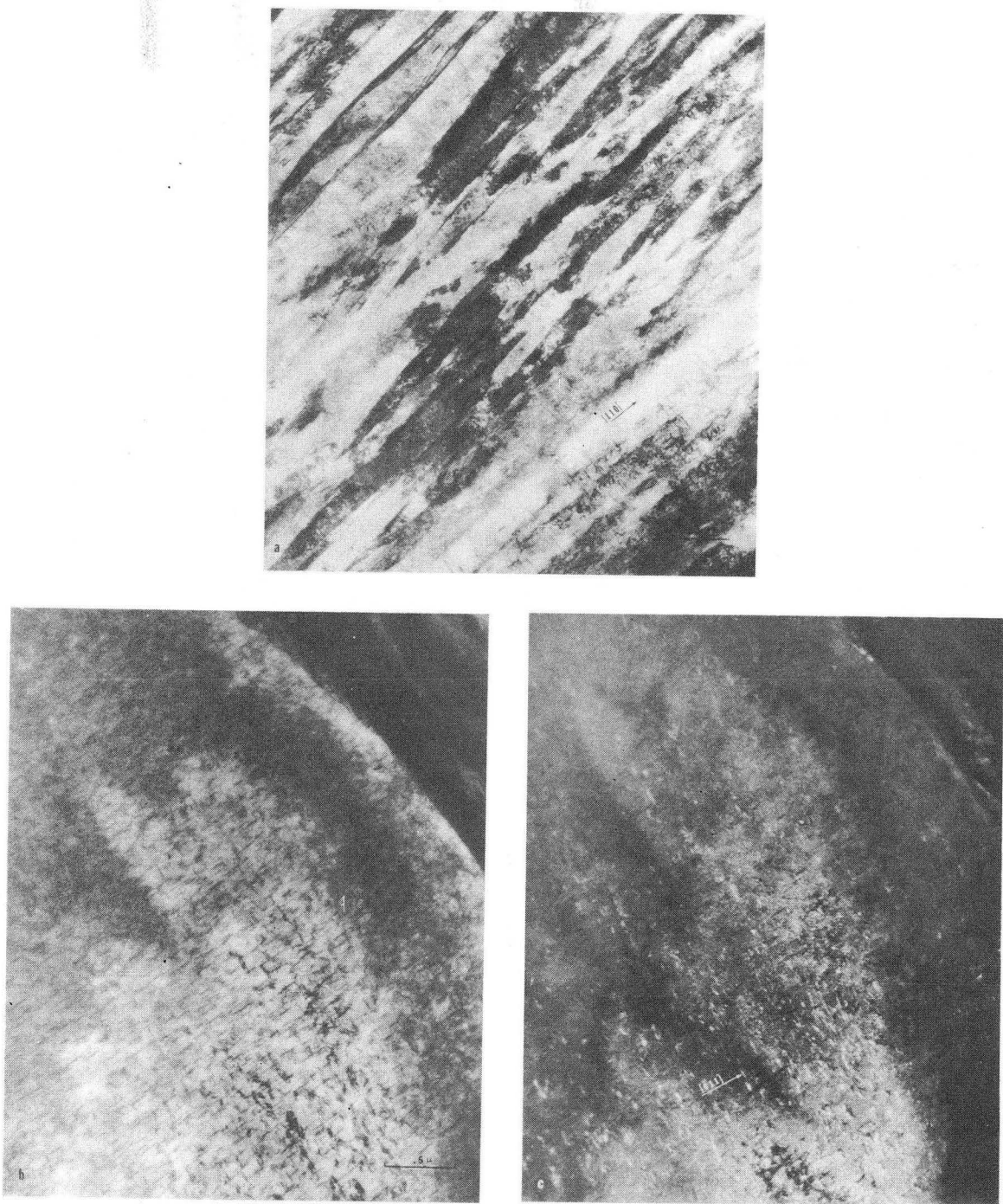
XBB 736-3529

Fig. 5. Bright field micrographs (a,b) of typical as-quenched structure in alloy C198. Extensive auto-tempering is evident. Dark field (c) lights up one variant of auto-tempered Fe_3C seen in bright field (b). Foil orientation: (a) (111); (b,c) (100)
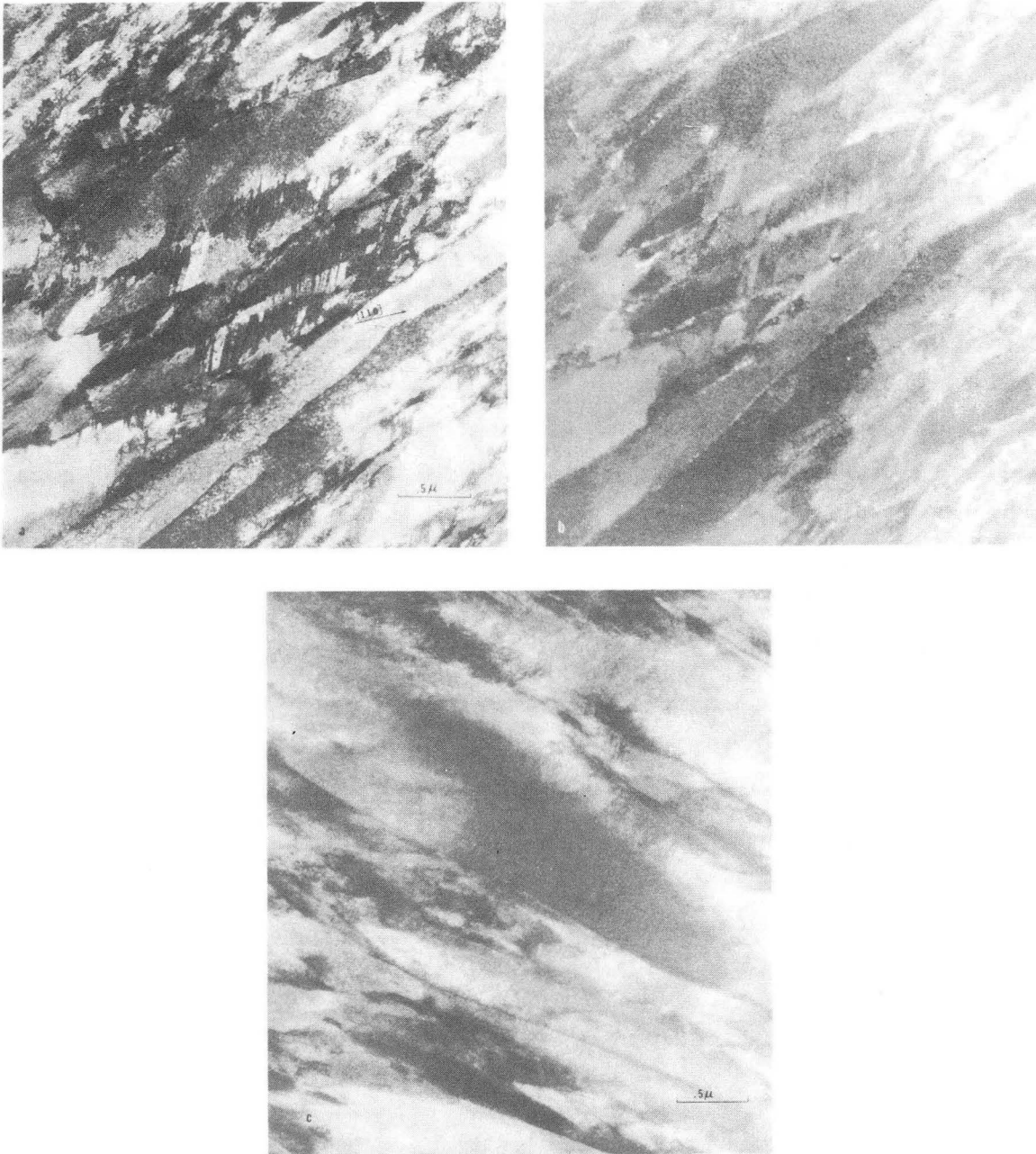
XBB 736-3521

Fig. 6. Bright field (a) and dark field (b) of typical as-quenched
microstructure in alloy C214. Dark field (b) lights up
Fe_3C interlath carbide present. Comparing bright field
micrographs (a,c) shows variation of percent twinning
observed in different regions of the same foil. Foil
orientation: (a,b) (111).
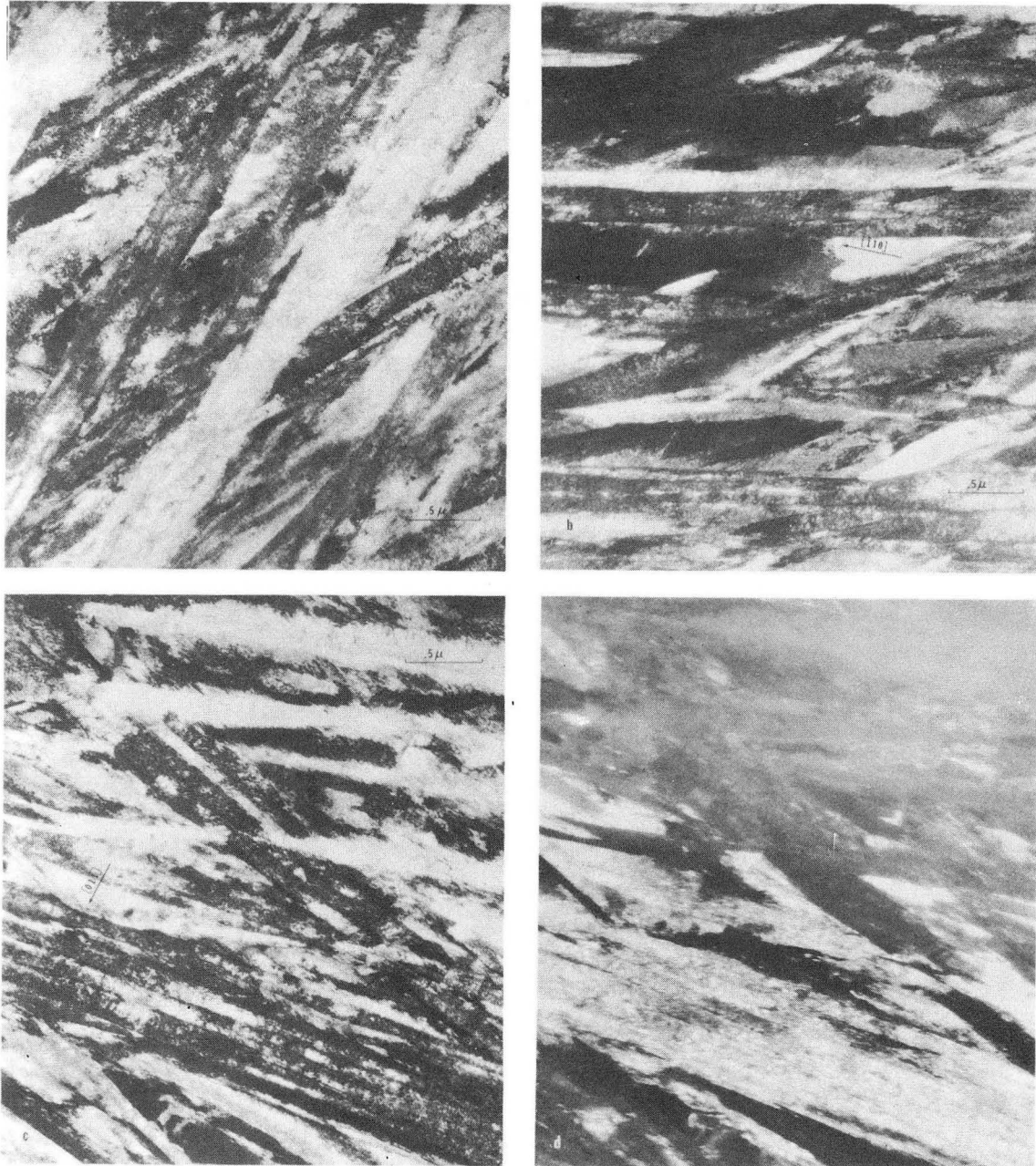
XBB 736-3530

Fig. 7. Bright field (a,b,c) micrographs of typical as-quenched
microstructures in alloy C215. Fine packets of lath martensite
are visible in bright field (c) and one such packet is lit up
in dark field (d). Foil orientations: all (111).
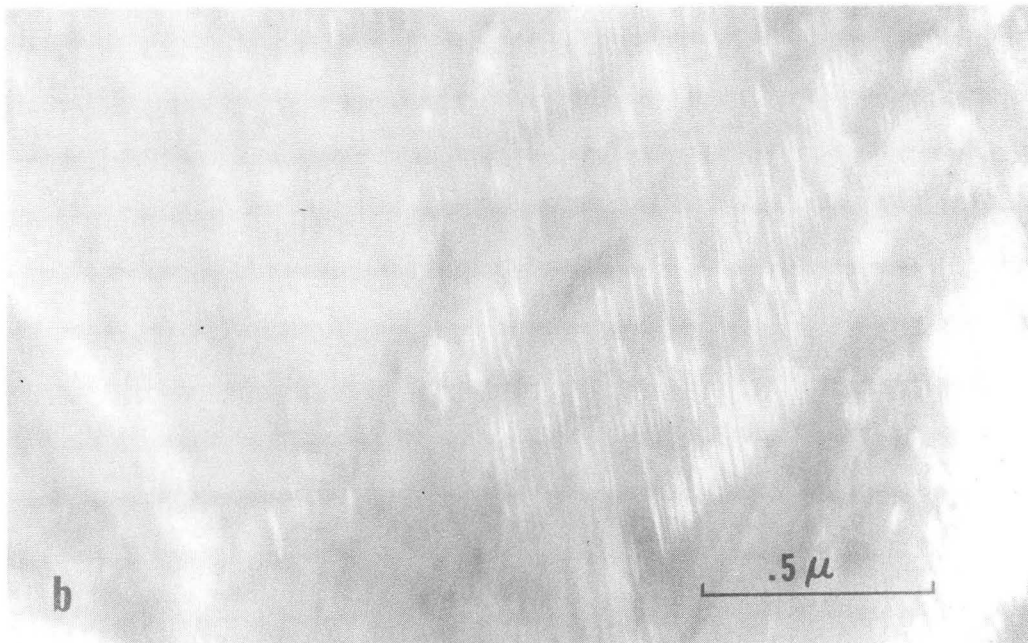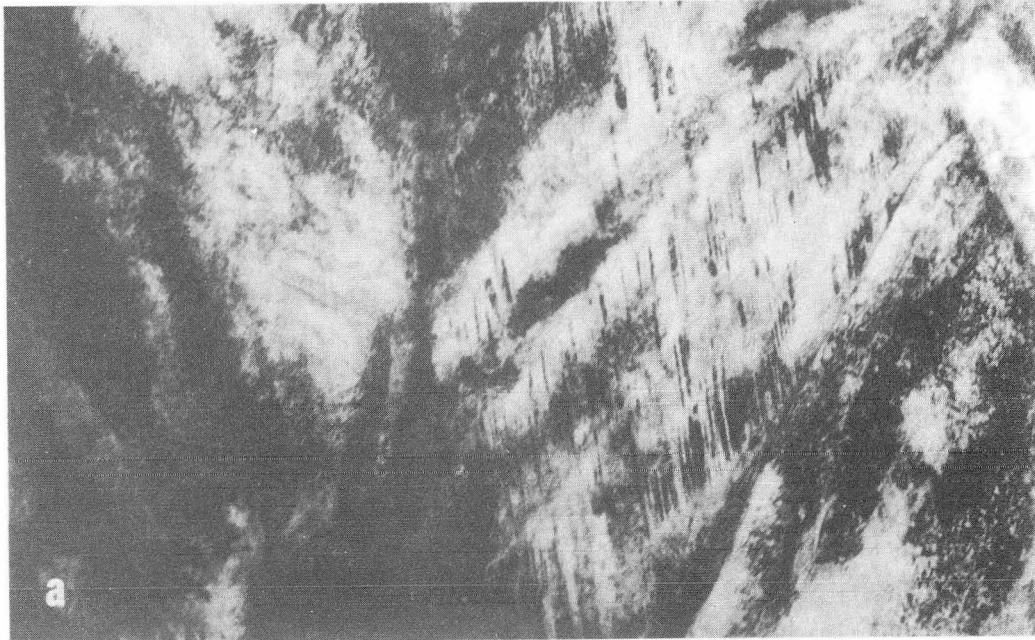
XBB 736-3517

Fig. 8. Bright field (a) and dark field of twins (b) in a heavily
twinned region in as-quenched alloy 215.
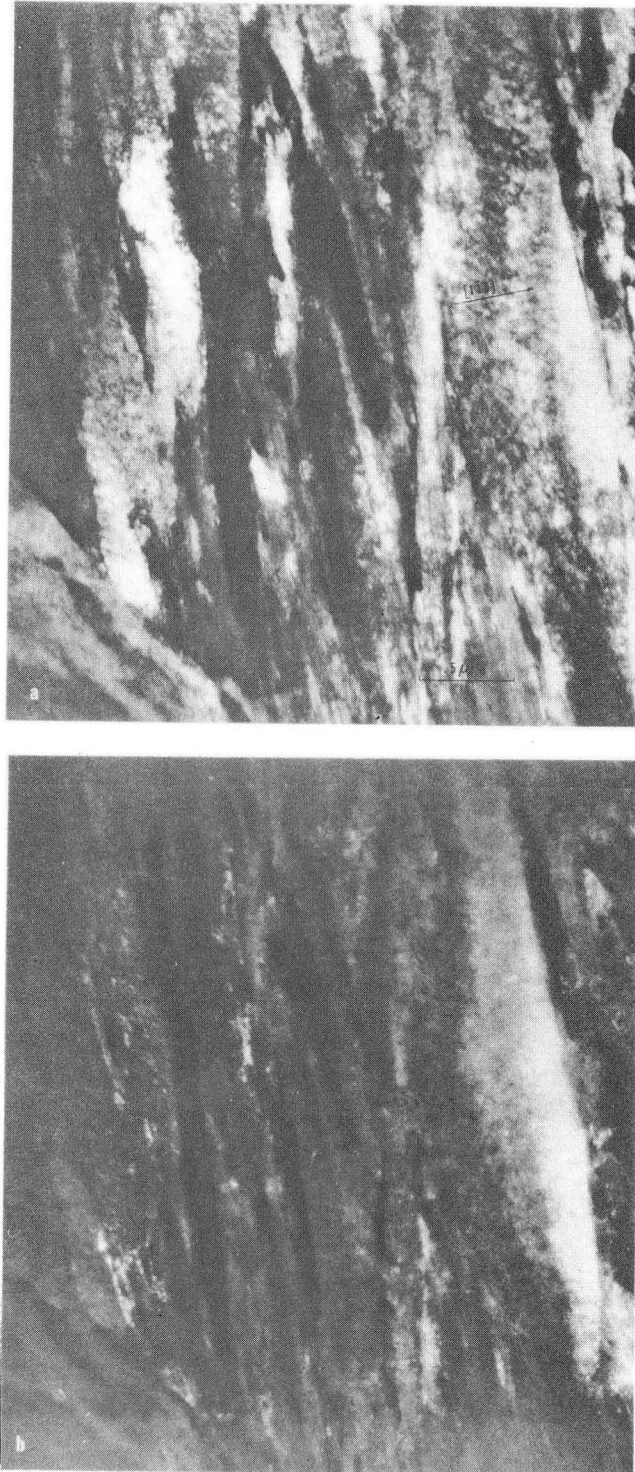
XBB 736-3522

Fig. 9. Bright field (a) and dark field showing typical Fe₃C distribution (b) in as-quenched alloy 216. Foil orientation
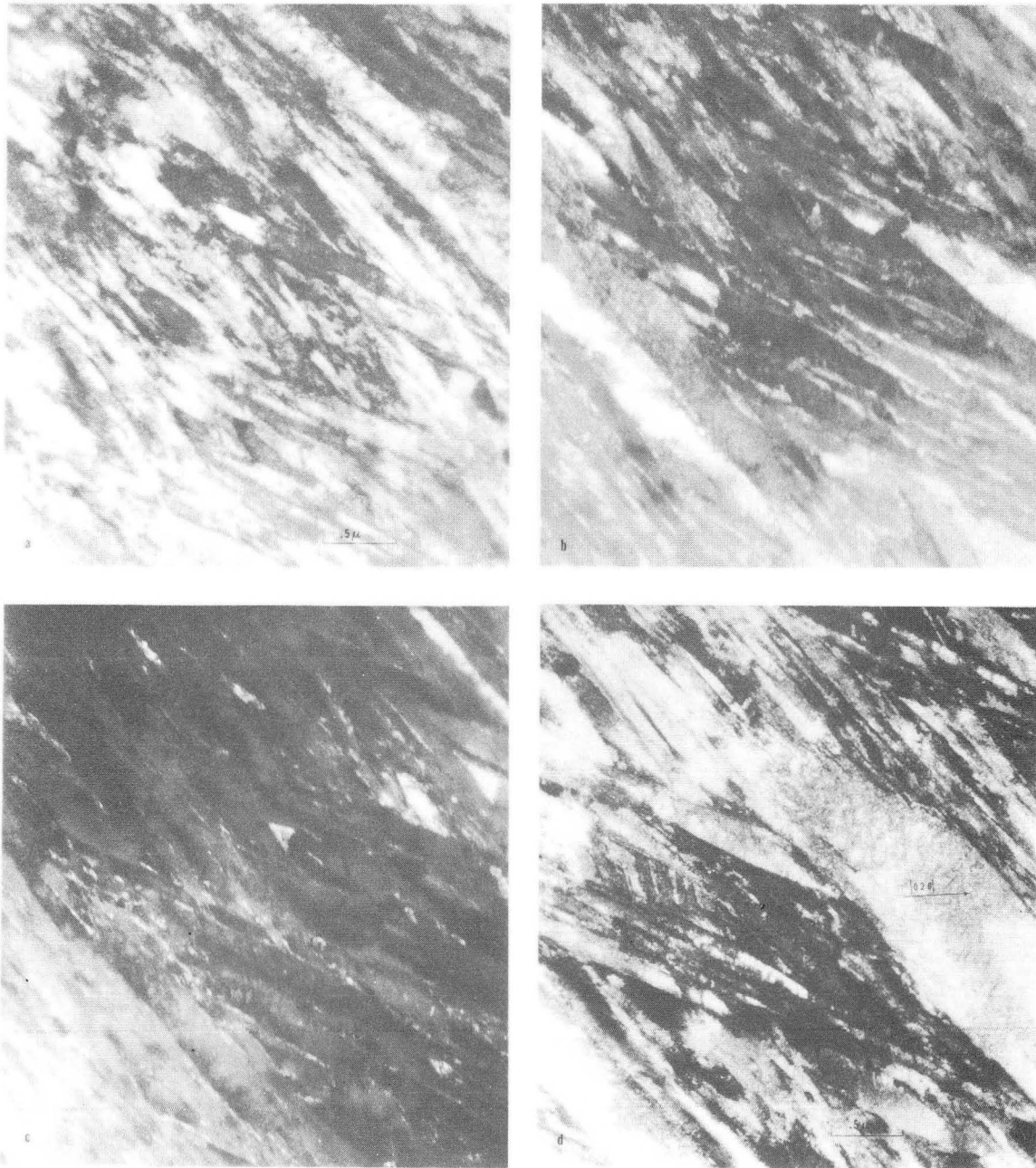
XBB 736-3527

Fig. 10. Bright field (a) and dark fields showing heavy interlath Fe$_3$C
precipitation (b,c) in typical as-quenched microstructure of
alloy 217. Bright field (d) shows another region of this
microstructure. Foil orientations (a,b,c) (111); (d) (100).

-45-
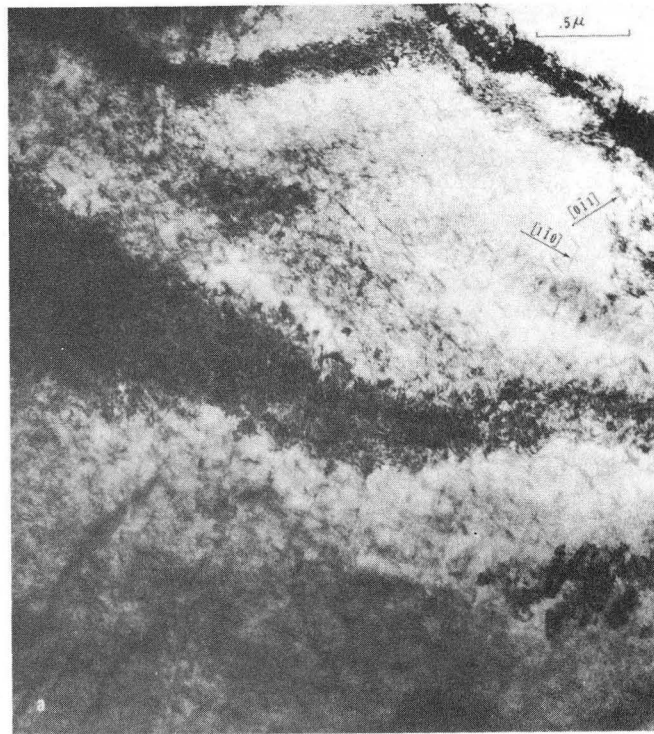
Fig. 11. Bright field micrographs showing continued precipitation
and growth of Widmanstatten Fe_3C (a) and the existence
of twins (b) in alloy C198 tempered at 400°C. Foil
orientation: (a) (111).
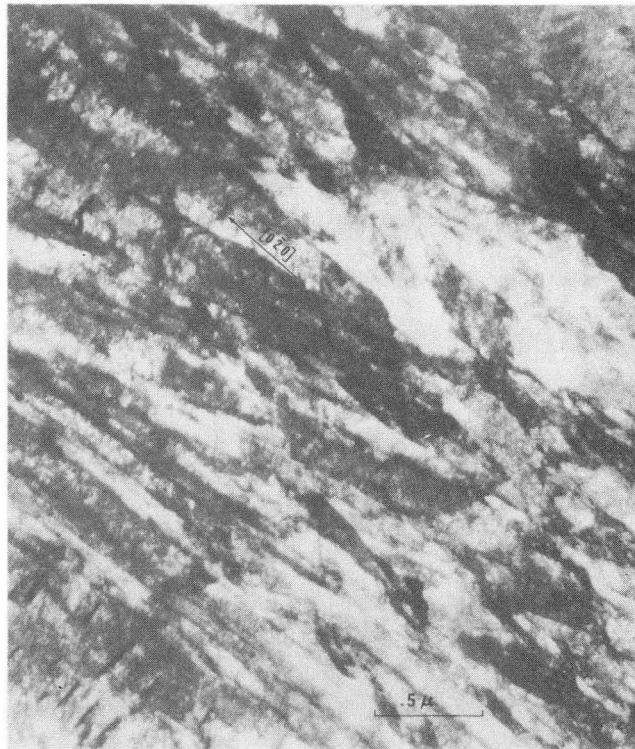
XBB 736-3519

Fig. 12. Bright fields (a,b) of typical microstructure in alloy 214 tempered at 400°C. Observe presence of large Fe_3C precipitates. Foil orientation: (a) (100); (b) (311).
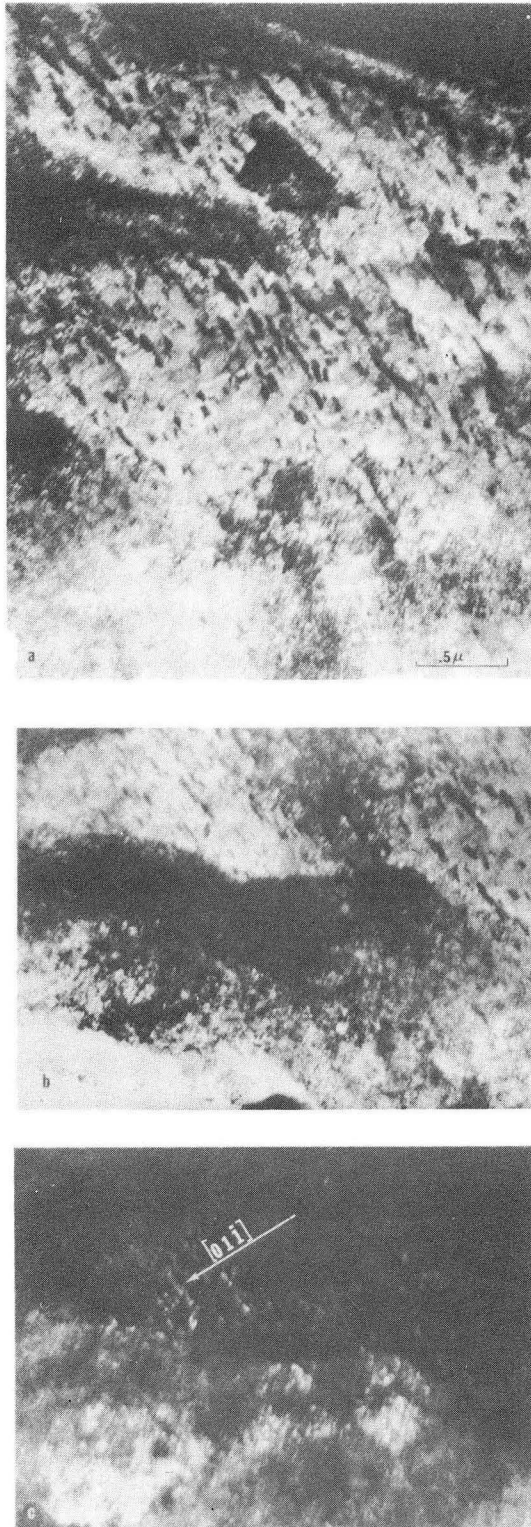
XBB 736-3525

Fig. 13. Typical microstructures present in alloys 215 and 217
tempered at 400°C. Large spherodized carbides are seen in the
bright field micrographs (a,b). Dark field (c) lights up the
Fe_3C precipitate shown in bright field (b). Foil orientation:
(111).
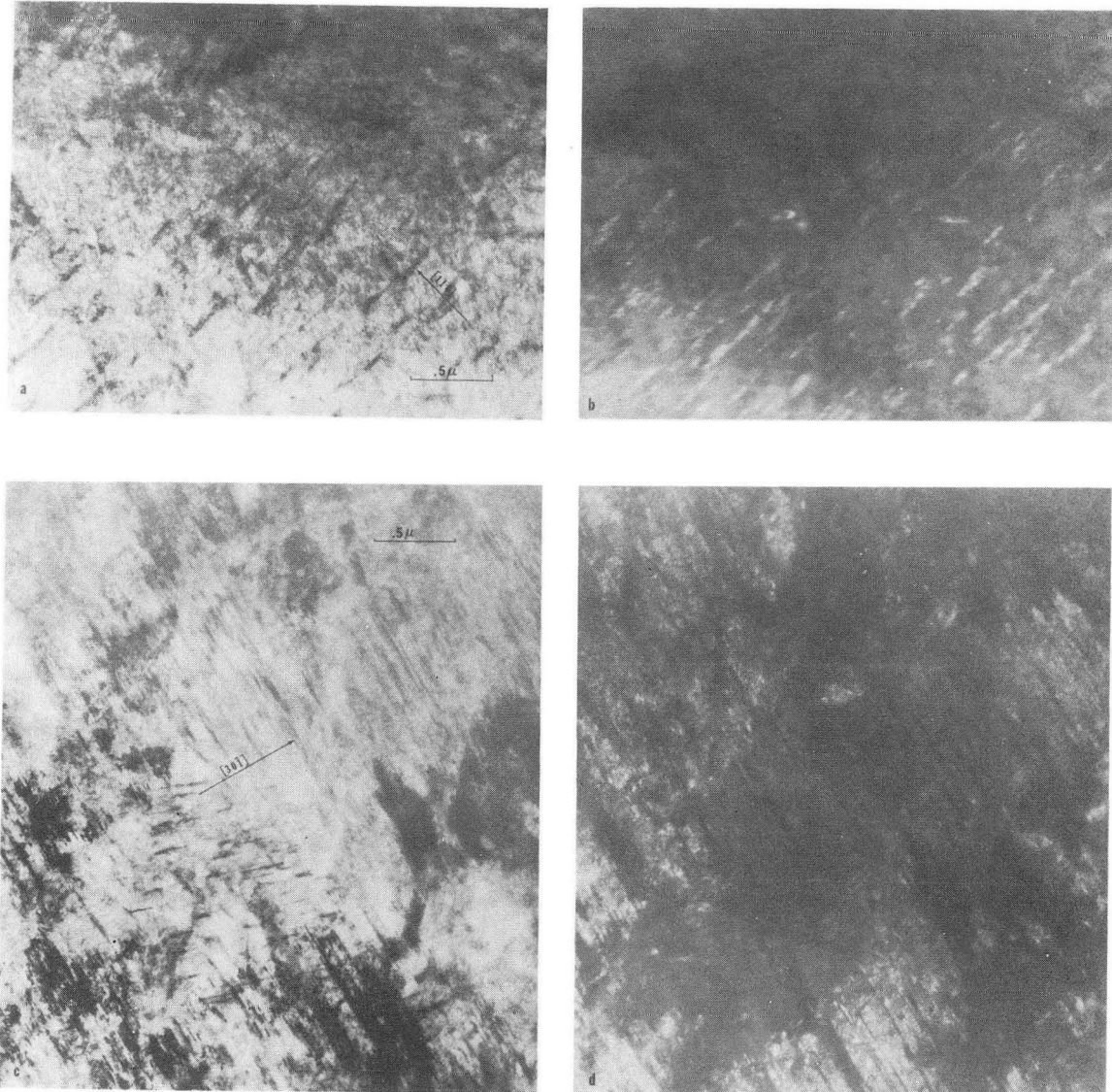
XBB 736-3518

Fig. 14. Typical microstructures present in alloy 216 tempered at
400°C. Bright field (a) and dark field of large Fe_3C
precipitates (b) present through much of structure. Bright
field of heavily twinned region (c) and dark field of
carbide formed on twin boundaries (d). Foil orientation:
(c,d) (133).
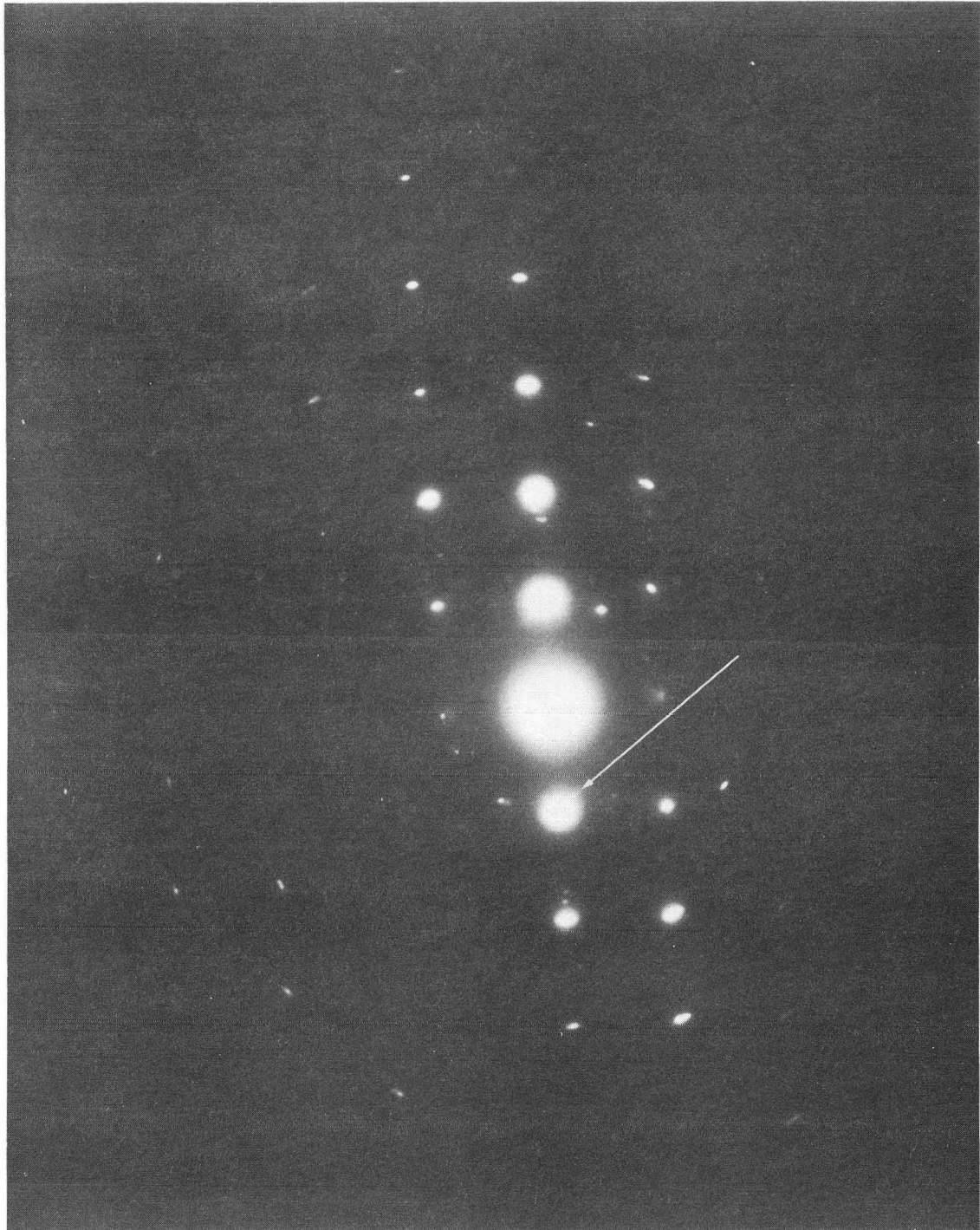
XBB 736-3523

Fig. 15. Selected area diffraction of pattern with arrow pointing to
streak indicative of Mo_2C precipitate. Such streaking found
in diffraction patterns of all alloys tempered at 600°C.
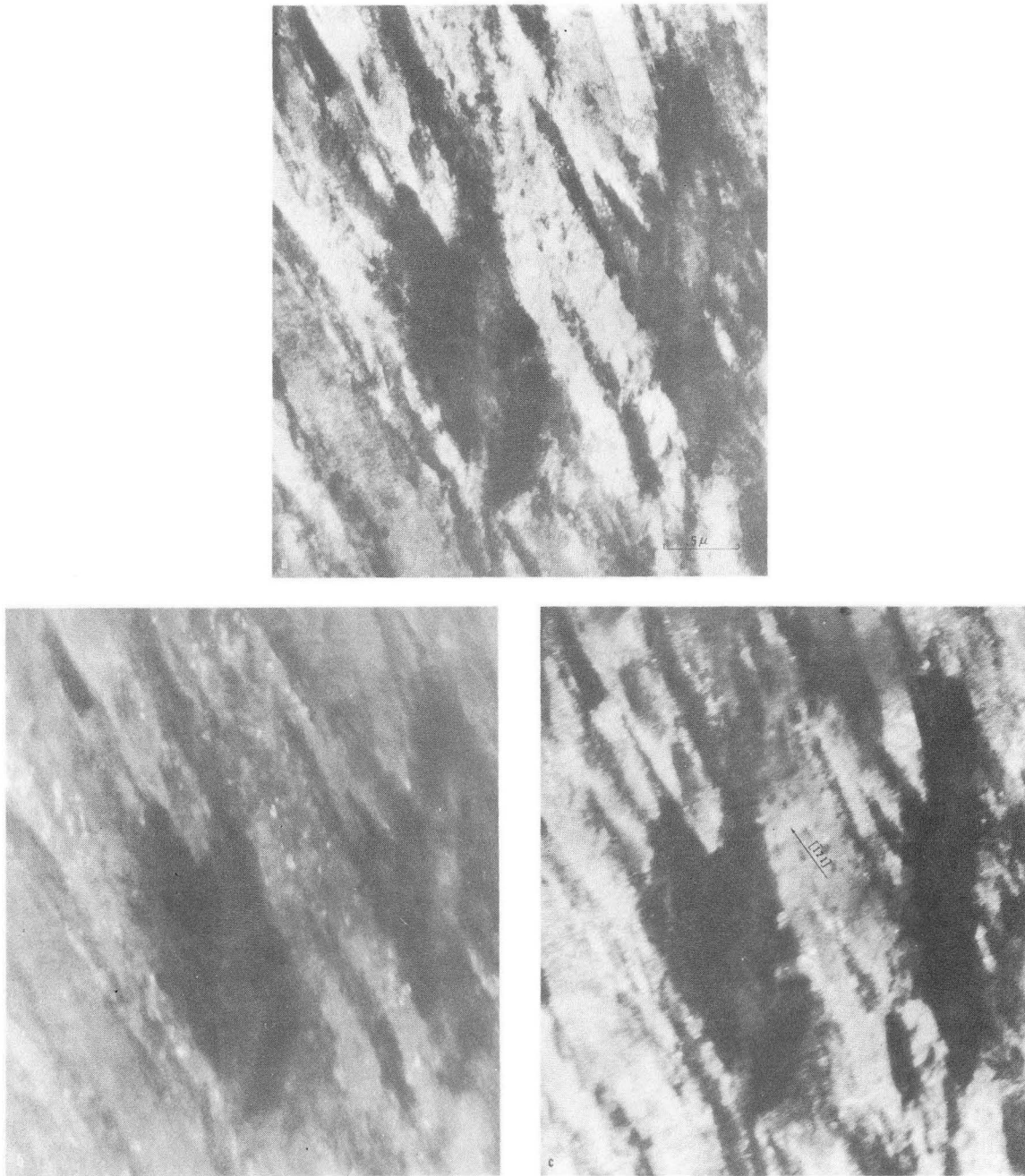
XBB 736-3528

Fig. 16. Bright field (a), dark field of a cementite spot (b), and dark
field of an Mo$_2$C streak (c) showing characteristic carbide
distributions in low molybdenum alloys tempered at 600°C.
Alloy 217, foil orientation: (311).
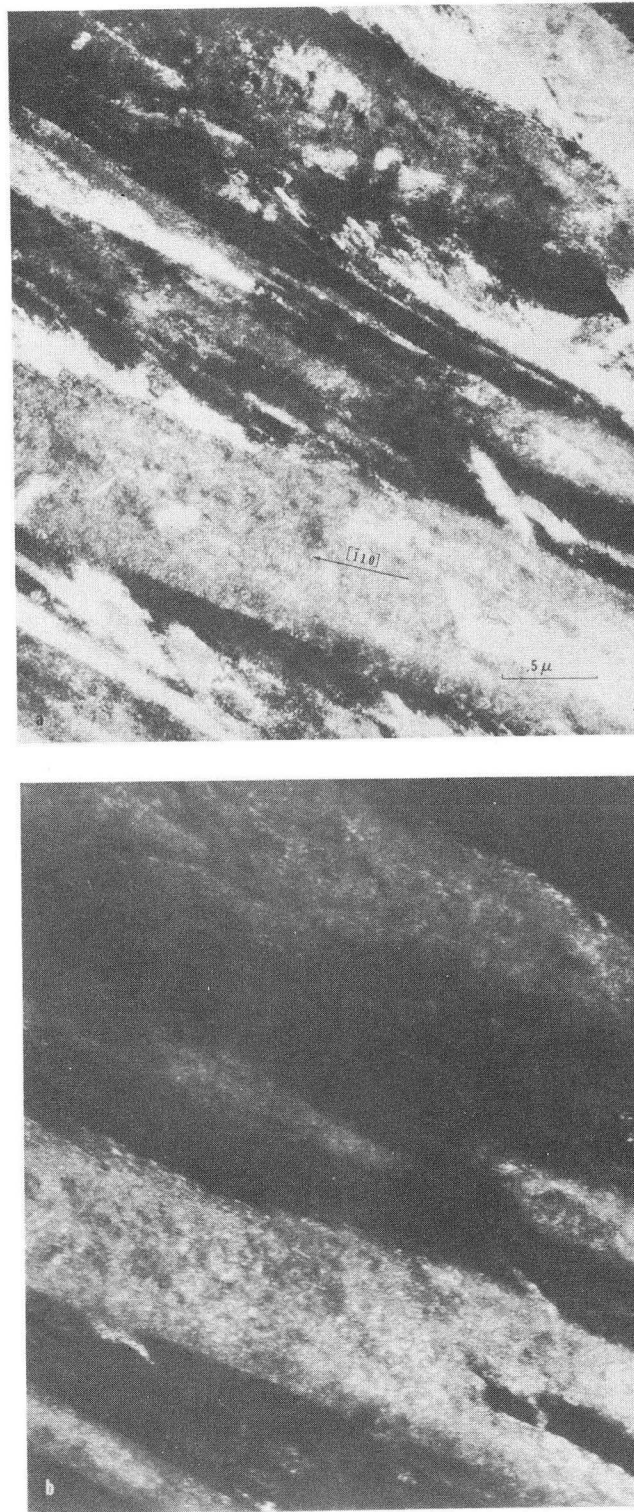
XBB 736-3516

Fig. 17. Typical appearence of Mo$_2$C precipitate. Bright field (a) and dark field of a Mo$_2$C streak (b). Alloy 215, foil orientation: (111).
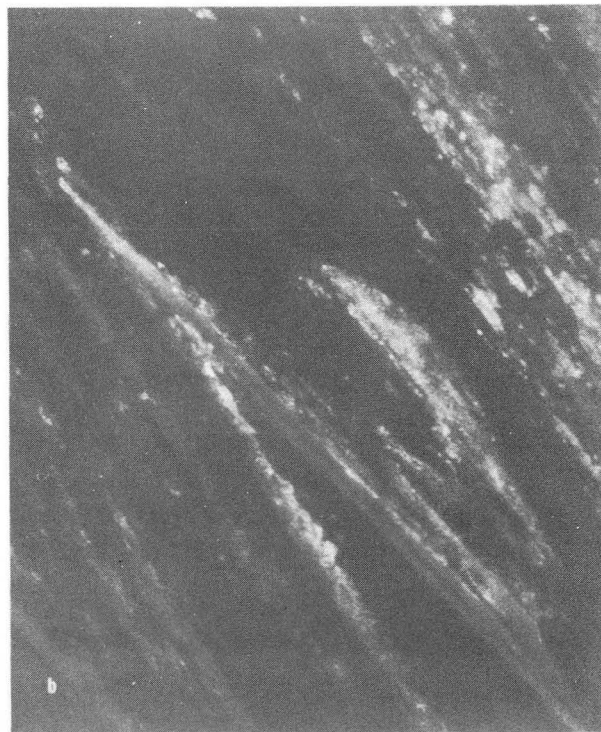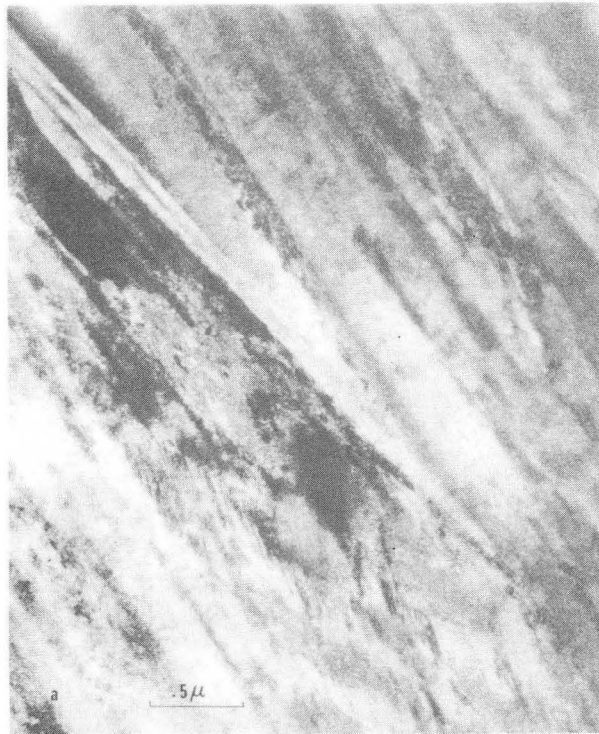
XBB 736-3520

Fig. 18. Bright field (a) and dark field of cementite spot (b),
showing characteristic Fe_3C distribution in high
molybdenum alloys tempered at 600°C. Alloy 215.
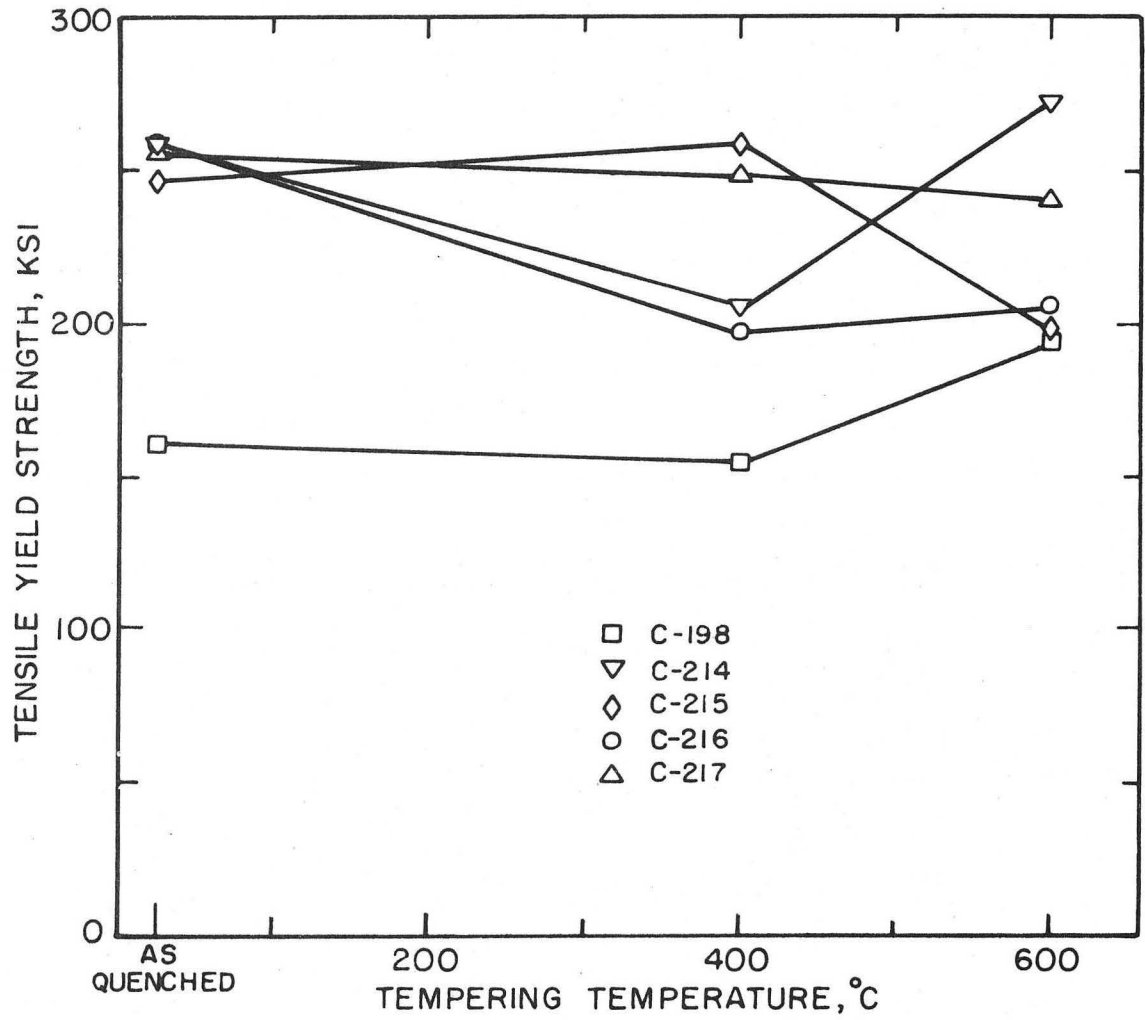
XBL 735-6192

Fig. 19. Room temperature tensile yield strength (0.2% offset) as
a function of tempering temperature.
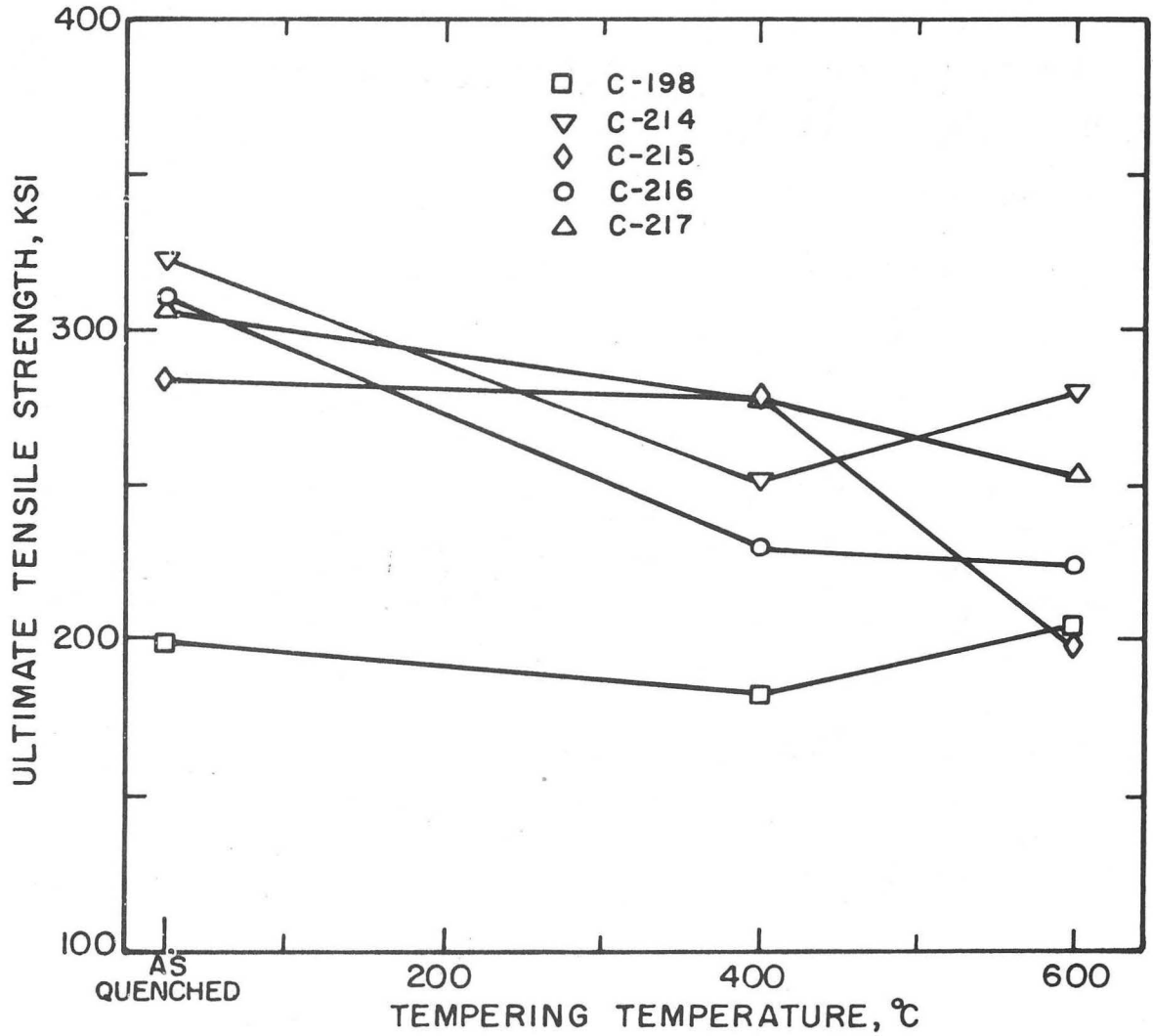
XBL 735-6193

Fig. 20. Room temperature ultimate tensile strength as a function of
tempering temperature.
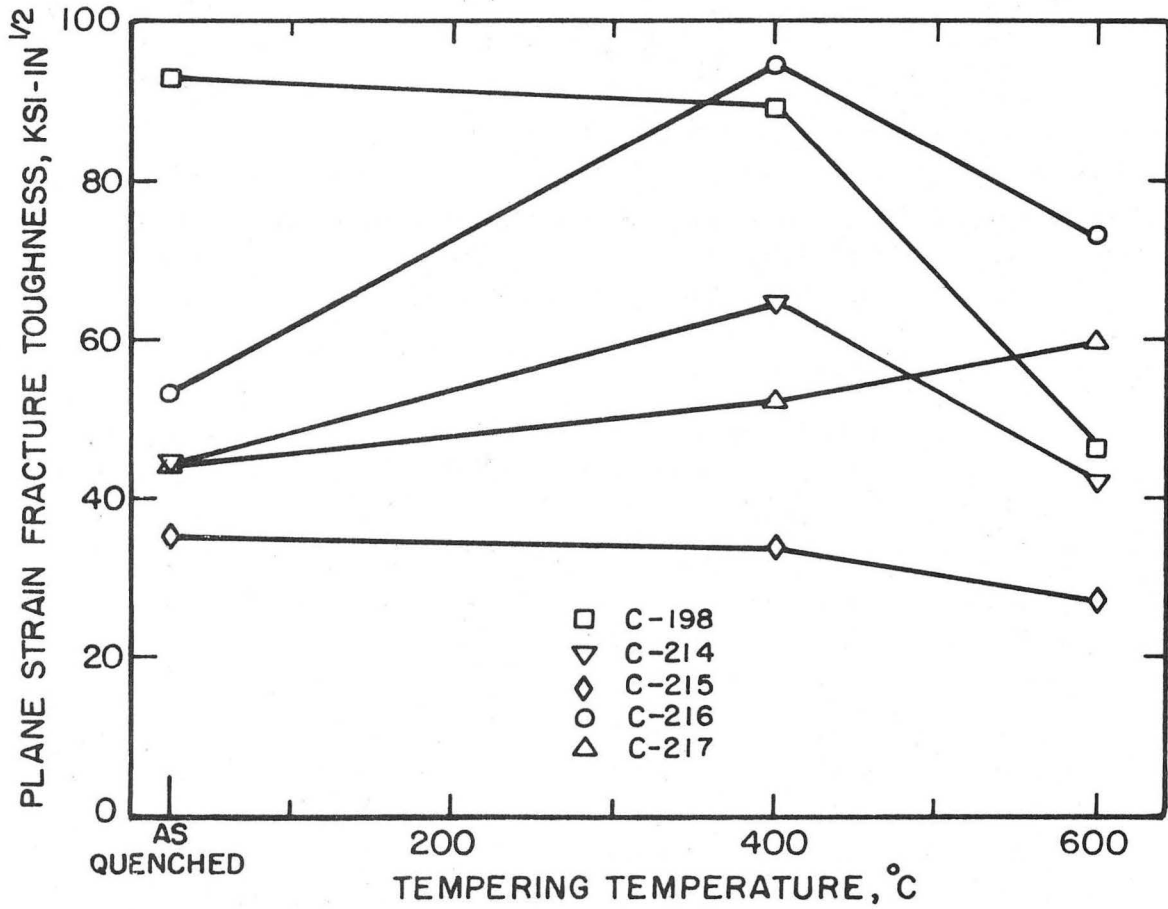
XBL 735-6194

Fig. 21. Room temperature plane-strain fracture toughness as a
function of tempering temperature.
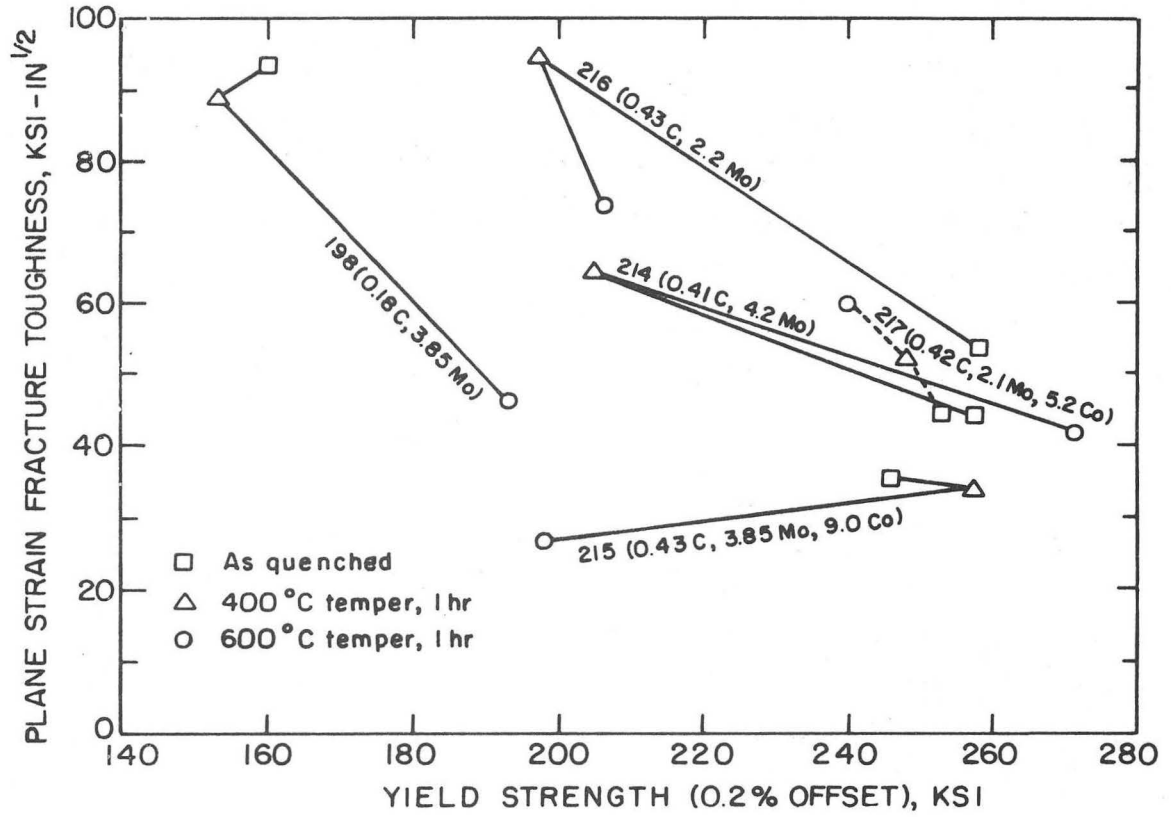
XBL 732-5719

Fig. 22. Room temperature plane-strain fracture toughness vs
tensile yield strength for each of the tempering
conditions.
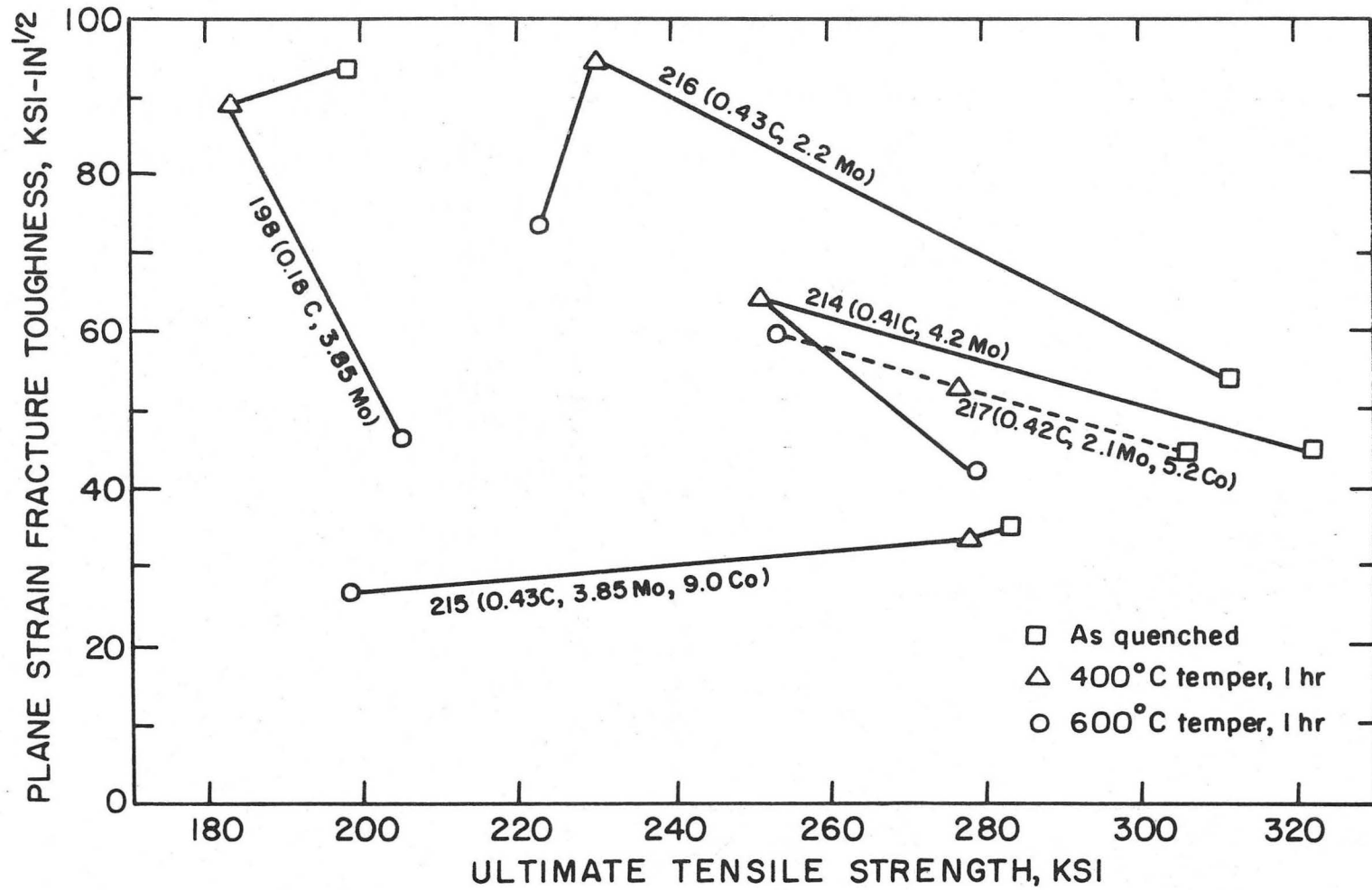
Fig. 23. Room temperature plane-strain fracture toughness vs ultimate tensile strength for each of the tempering conditions.
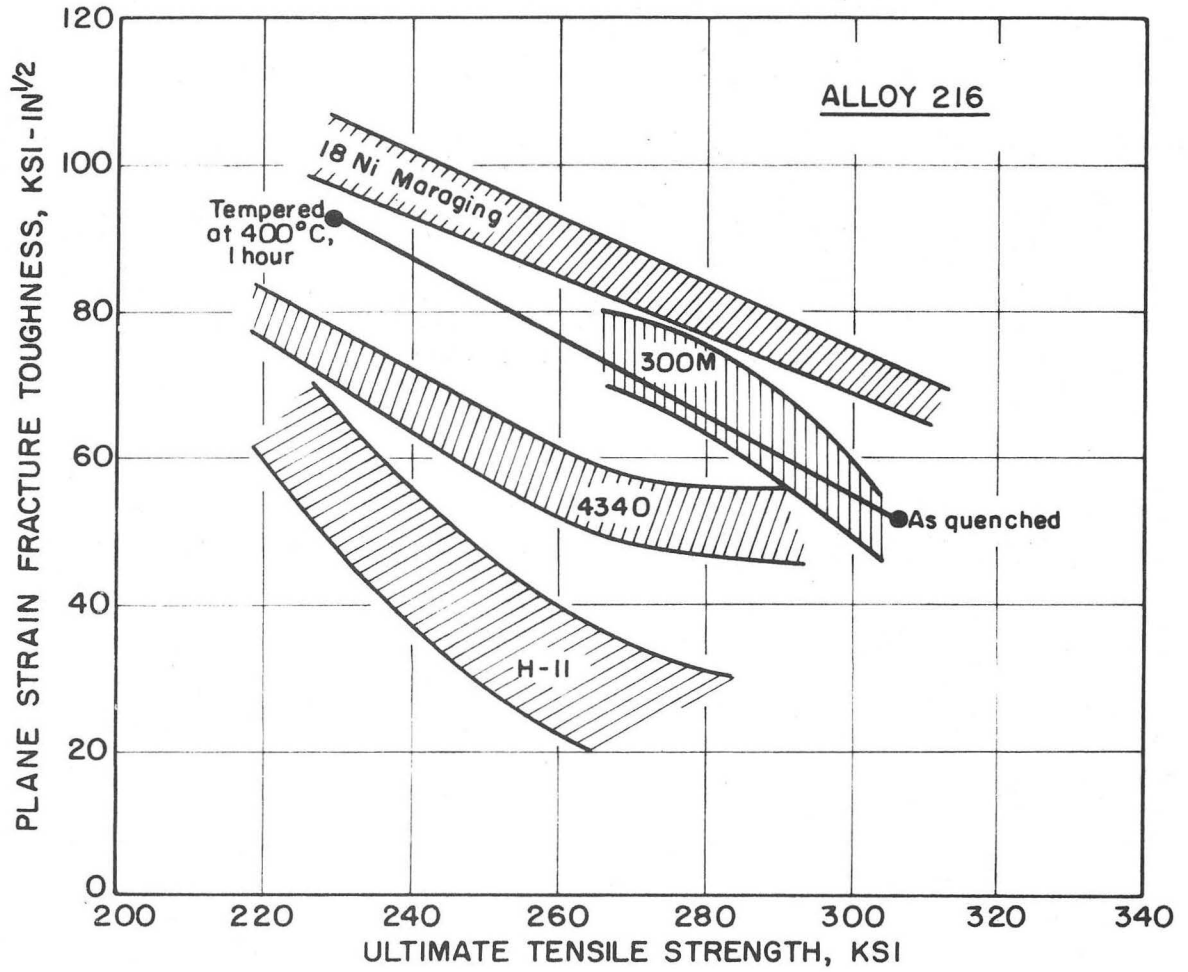
XBL 732-5717

Fig. 24. Comparison of ultimate tensile strength and plane strain
fracture toughness of alloy 216 with the strength and
toughness properties of several ultrahigh-strength
commercial steels.
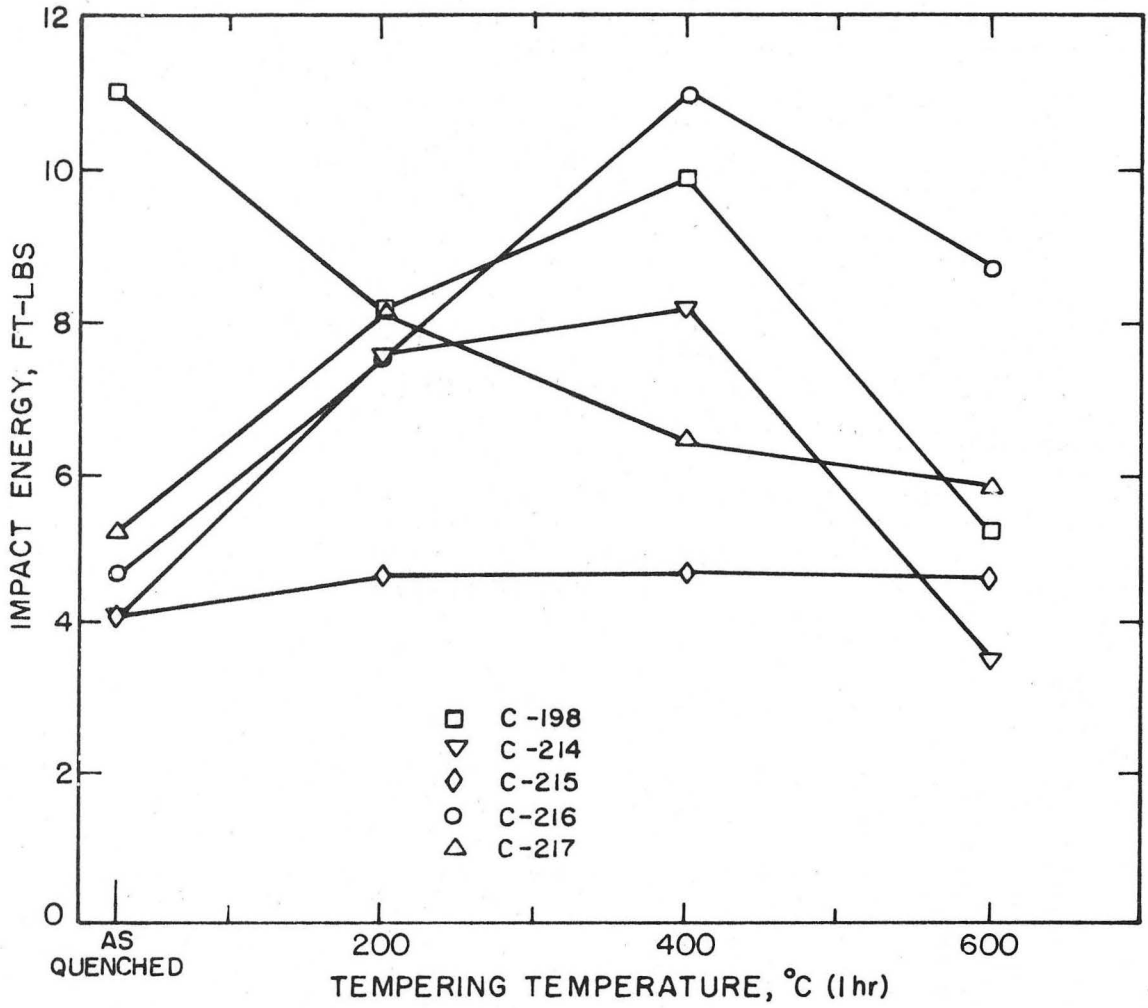
Fig. 25. Room temperature Charpy-impact energy as a function of tempering temperature.
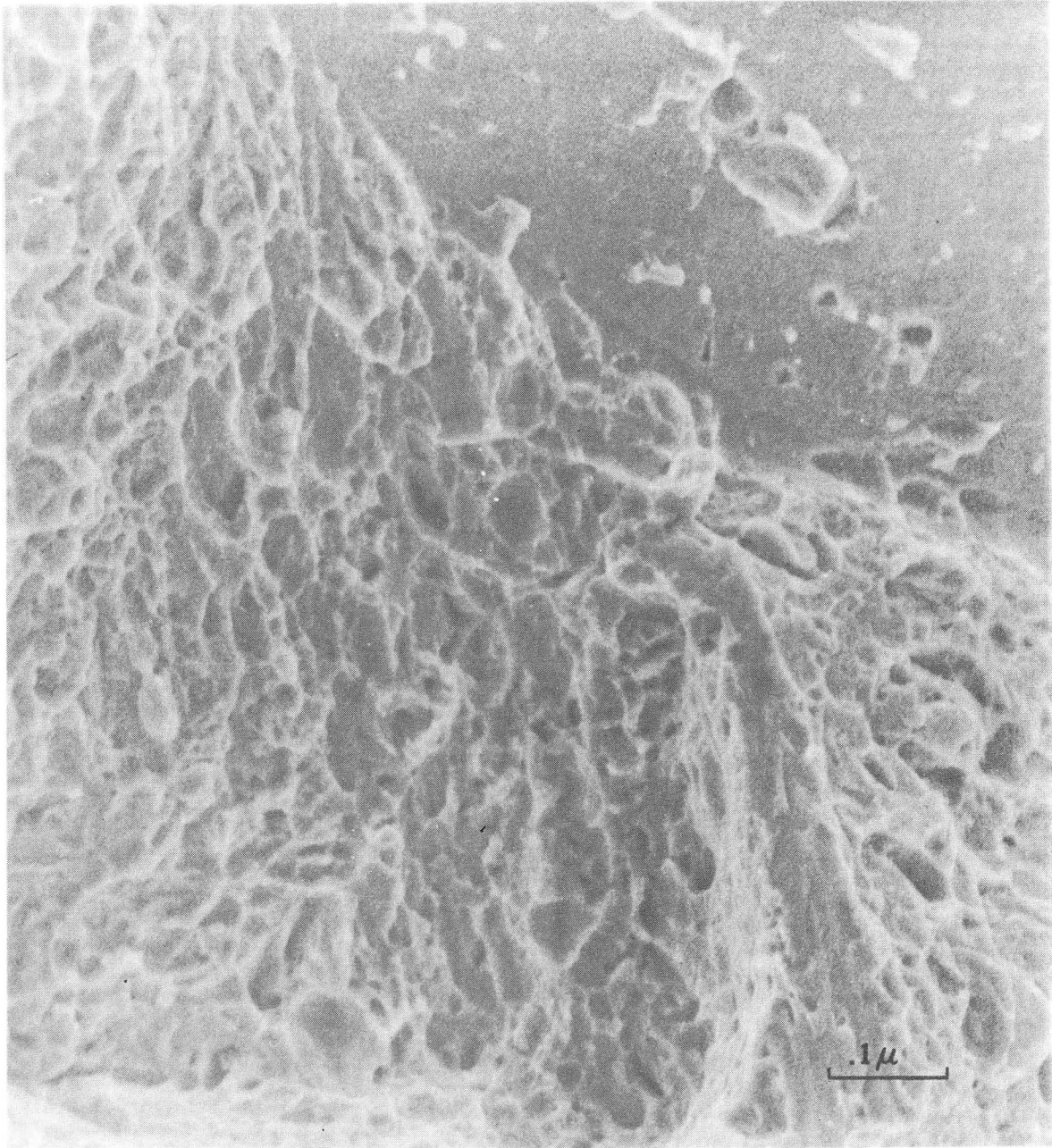
XBB 736-3524

Fig. 26. Scanning electron micrograph showing typical fracture surface
exhibited by all fracture toughness specimens. The fracture
surface is a mixture of low level dimples mixed with varying
amounts of flat cleavage areas.